Dally is not essential for Dpp spreading or internalization but for Dpp stability by antagonizing Tkv-mediated Dpp internalization

Niklas Simon*[1], Abu Safyan *[2,3,4,5,6], George Pyrowolakis[,3,4,5,6], Shinya Matsuda[1]

1. Growth & Development, Biozentrum, Spitalstrasse 41, University of Basel, 4056 Basel, Switzerland
2. International Max Planck Research School for Immunobiology, Epigenetics, and Metabolism, Freiburg, Germany.
3. Institute for Biology I, Faculty of Biology, University of Freiburg, Freiburg, Germany.
4. CIBSS – Centre for Integrative Biological Signalling Studies, University of Freiburg, Freiburg, Germany.
5. BIOSS – Centre for Biological Signalling Studies, University of Freiburg, Freiburg, Germany.
6. Hilde Mangold Haus, University of Freiburg, Habsburgerstrasse 49, 79104 Freiburg, Germany.

* These authors contributed equally.

For correspondence:
shinya.matsuda@unibas.ch
g.pyrowolakis@biologie.uni-freiburg.de

Abstract

Dpp/BMP acts as a morphogen to provide positional information in the Drosophila wing disc. Key cell-surface molecules to control Dpp morphogen gradient formation and signaling are heparan sulfate proteoglycans (HSPGs). In the wing disc, two HSPGs, the glypicans Division abnormally delayed (Dally) and Dally-like (Dlp) have been suggested to act redundantly to control these processes through direct interaction of their heparan sulfate (HS) chains with Dpp. Based on this assumption, a number of models on how glypicans control Dpp gradient formation and signaling have been proposed, including facilitating or hindering Dpp spreading, stabilizing Dpp on the cell surface, or recycling Dpp. However, how distinct HSPGs act remains largely unknown. Here we generate genome-engineering platforms for the two glypicans and find that only Dally is critical for Dpp gradient formation and signaling through interaction of its core protein with Dpp. We also find that this interaction is not sufficient and the HS chains of Dally are essential for these functions largely without interacting with Dpp. We provide evidence that the HS chains of Dally are not essential for spreading or recycling of Dpp but for stabilizing Dpp on the cell surface by antagonizing receptor-mediated Dpp internalization. These results provide new insights into how distinct HSPGs control morphogen gradient formation and signaling during development.

Introduction

Morphogens are signaling molecules secreted from localized source cells to control cell fates in a concentration dependent manner during development [1-4]. Amongst them, Decapentaplegic (Dpp), the vertebrate BMP2/4 homolog is the first validated secreted morphogen identified in Drosophila. Since its discovery, the role of Dpp signaling in the Drosophila wing imaginal disc (the larval precursor of the adult wing) has served as an excellent model to investigate how morphogen gradients form and act [5-7]. In the wing disc, Dpp is expressed in an anterior stripe of cells along the anterior-posterior compartment boundary to control nested target gene expression and tissue growth (Fig. 1A). Dpp binds to the type I receptor Tkv and the type II receptor Punt to induce the phosphorylation of the transcription factor Mad. Phosphorylated Mad (pMad) forms a complex with the co-Smad (Medea) to accumulate into the nucleus and activate or inhibit target gene transcription. Interestingly, the majority of Dpp target genes are repressed by the transcriptional repressor Brinker (Brk) while pMad directly represses *brk* expression [8-10]. Thus, the pMad gradient regulates nested target gene expression mainly through generating an inverse gradient of Brk [11] (Fig. 1A). The nested target gene expression patterns are thought to position the future adult wing veins such as L2 and L5 [12,13] (Fig. 1A). In addition to patterning, Dpp signaling controls growth of the wing through repressing Brk as the strong proliferation defects of *dpp* mutant wing discs can be reversed by removing *brk* [8,14].

While endogenous Dpp is indeed distributed in a graded manner [15], how the gradient arises is highly controversial [6,7,16]. A class of molecules that control gradient formation of various morphogens are glypicans, GPI-anchored heparan sulfate proteoglycans (HSPGs) consisting of a core protein and covalently attached heparan sulfate (HS) chains [17,18 19]. In Drosophila, two glypicans, Division abnormally delayed (Dally) [20] and Dally-like protein (Dlp) [21], are thought to redundantly act as co-receptors [22], regulate Dpp morphogen gradient formation [23,24], and control scaling of Dpp gradient with tissue size [25,26].

The role of glypicans in Dpp signaling is dependent on HS chains. A variety of genes required for HS chain biosynthesis such as *sulfateless* (*sfl*) and a family of Ext genes (*sister of tout-velu* (*sotv*), *brother of tout-velu* (*botv*), and *tout-velu* (*ttv*)) [27-29] have been shown to be involved in Dpp distribution and signaling. Given that Dpp binds to heparin [30], the interaction of the HS chains of glypicans with Dpp is thought to be essential for their function.

Several, not necessarily mutually exclusive, models have been proposed on how glypicans control Dpp morphogen gradient formation. First, glypicans are suggested to be essential for Dpp spreading by handing it over from one cell to the next cell in a “bucket brigade” manner (“facilitated diffusion” model) [31] (Fig. 1B). Consistently, FRAP assays using overexpression of GFP-Dpp revealed a low diffusion coefficient of Dpp ($D=0.1\mu m^2/s$) [32]. Indeed, pMad signal and Dpp distribution have been shown to be reduced not only in glypican mutant clones but also in wild type cells located adjacent to the clone and distally to the Dpp source (so-called “shadow” effect), indicating that Dpp spreading requires glypicans [23].

Second, and in contrast to the first model, glypicans have been proposed to interfere with Dpp spreading [33] (Fig. 1C). The “hindered diffusion” model postulates that Dpp spreads freely and transient interaction of Dpp with cell surface molecules such as glypicans hinders effective Dpp spreading [33].

Third, glypicans have been proposed to stabilize Dpp on the cell surface [30] (Fig. 1D). A previous study showed that Dpp lacking the N-terminal HS binding site is less stable than wild type Dpp [30], indicating that Dally regulates Dpp stability through interactions of HS chains with Dpp. Genetic analyses indicated that Dally competes with Tkv for Dpp binding to antagonize Tkv-mediated Dpp internalization [30].

Fourth, glypicans are proposed to control recycling and re-secretion of Dpp, which is critical for extracellular Dpp gradient scaling [25], a phenomenon in which the Dpp gradient expands to match the growing wing disc size during development (Fig. 1E). Surprisingly, although receptor-mediated endocytosis is thought to be a mechanism to clear morphogens from the extracellular space (Fig. 1D), the same study showed that Dpp internalization was not affected in *tkv* mutant clones, indicating that Dally, but not Tkv, mediates Dpp internalization [25].

Finally, a recent attempt to create a synthetic morphogen system using free diffusing GFP as a morphogen raises alternative possibilities [34]. When *dpp* was replaced with GFP, and anti-GFP nanobodies fused to Tkv and Punt that can activate pMad signal upon GFP binding were introduced, rescue of severe *dpp* mutant phenotypes was not perfect but improved by further introducing GPI-anchored non-signaling receptors (corresponding to glypicans). Supported by mathematical modeling, this study suggests that glypicans may contribute to morphogen gradient formation by blocking morphogen leakage and assisting morphogen spreading likely via their GPI-anchors [34].

Previously, we generated a platform to introduce epitope tags and/or mutations in the *dpp* locus and protein binder tools to directly manipulate endogenous Dpp spreading [15]. By visualizing and manipulating the endogenous Dpp morphogen gradient, we found that Dpp spreading is critical for posterior patterning and growth but largely dispensable for anterior patterning and growth [15]. Although the requirements for Dpp spreading were thus less important than previously thought, the endogenous Dpp gradient was easily visualized in the wing discs and Dpp spreading was still critical for posterior patterning and growth [15]. Thus, wing imaginal discs serve as an excellent model to study Dpp dispersal-mediated morphogen gradient formation at physiological conditions.

In this study, to better understand how glypicans control Dpp morphogen gradient formation and signaling, we generated genome-engineering platforms to manipulate both Drosophila glypicans, Dally and Dlp. Although the two glypicans are thought to act redundantly, we first find that only Dally is critical for Dpp gradient formation through interaction of its core protein with Dpp. Surprisingly, we found that, although the HS chains of Dally are essential for Dally's function, *dpp* mutants that lack the interaction with HS chains display only minor phenotypes, indicating that the direct interaction of HS chains of Dally with Dpp is largely dispensable for Dpp gradient formation and signaling. We provide evidence that the HS chains of Dally are not essential for Dpp internalization or spreading but rather stabilize Dpp on the cell surface by antagonizing Tkv-mediated internalization of Dpp. These results provide new insights into how glypicans control dispersal and signaling of distinct morphogens during development.

Results

Dally but not Dlp interacts with Dpp

Previous genetic studies suggested that both Dally and Dlp are involved in extracellular Dpp distribution and signaling through the interaction of Dpp with their HS chains [23]. However, the relative contribution of each glypican remained unclear. To address this, we first expressed *dally* or *dlp* in the dorsal compartment of the wing disc using *ap*-Gal4 to compare their ability to interact with endogenous Dpp and activate pMad signal *in vivo*. To visualize endogenous extracellular Dpp distribution, we utilized a functional *Ollas-dpp* allele [35]. Since Dpp distribution and pMad signal are similar between the dorsal and ventral compartments in *Ollas-dpp* discs (Fig. S1), the ventral compartment serves as an internal control in this assay. We found that expression of *dally* in the dorsal compartment increased HS chain levels, and expanded the extracellular Dpp distribution and pMad gradient compared to the control ventral compartment (Fig. 2A, B, E, F). Interestingly, despite the broad extracellular Ollas-Dpp accumulation, the pMad signal dropped to background levels at the lateral regions (Fig. 2E, F), indicating that Dpp signal activation by Dally is inefficient likely due to sequestration of Dpp by overexpressed Dally. In contrast, expression of *dlp* using *ap*-Gal4 increased HS chain levels but rather reduced extracellular Ollas-Dpp distribution and pMad gradient in the dorsal compartment compared to the control ventral compartment (Fig. 2C, D, G, H), likely because ectopic Dlp expression sequestered HS (Fig. 2C) and blocked HS modification of Dally. Consistent with a previous report [36], Dlp expression, in the dorsal compartment efficiently expanded extracellular Wg distribution compared to

Dally expression (Fig. S2). These results suggest that, although both Dally and Dlp are modified by HS chains, only Dally interacts with Dpp.

Dally, but not Dlp, is required for the Dpp activity gradient

To compare the requirement of Dally and Dlp for Dpp signaling gradient formation, we generated null mutants for *dally* and *dlp* (*dally*^{KO} and *dlp*^{KO} respectively) by replacing the first exon of each gene by an attP cassette via genome engineering (Fig. S3). Although there is no good anti-Dally antibody, defects in pMad signal in *dally*^{KO} wing discs were similar to that of *dally*^{MH32} (a *dally* null allele [37]) wing discs (Fig. 3A-C, I) and *dally*^{KO} adult wings showed similar phenotypes to *dally*^{MH32} adult wings (Fig. 3E-G, J). Immunostaining for Dlp revealed that Dlp expression is completely lost in *dlp*^{KO} wing disc (Fig. S4). Thus, we confirmed that both *dally*^{KO} and *dlp*^{KO} are null alleles. These null alleles also serve as a platform to insert epitope tags or modified versions of *dally* and *dlp* in the endogenous genomic locus via the attP cassette.

We then compared the two null alleles and found that, while severely shrunk in *dally*^{KO} wing discs, the pMad signal was not affected in *dlp*^{KO} wing discs (Fig. 3C, D, I). In rare-occurring mutant adult wings, patterning defects linked to defects in Dpp signaling (truncated L5) were only seen in *dally*^{KO} mutants (Fig. 3G). In contrast, the distance of the distal tips of L3 and L4 veins was reduced in *dlp*^{KO} mutants, which is indicative of Hh signaling defects (see arrows in Fig. 3H). Although both *dally*^{KO} and *dlp*^{KO} adult wings are smaller than controls (Fig. 3J), only *dally*^{KO} adult wings are narrower along the A-P axis, consistent with the role of Dpp along this axis (Fig. 3K).

It has been shown that *dally* and *dlp* display distinct expression patterns in the wing disc, since *dally* expression is controlled by Dpp signaling [24] and *dlp* expression is controlled by Wg signaling [36]. Thus, the differential expression pattern of Dally and Dlp may underlie the differential requirements of glypicans in Dpp signaling. To address this, we inserted *dlp* in the *dally* genomic locus using the attP site in the *dally*^{KO} allele, thus expressing *dlp* in the *dally* expression pattern. As a control, *YFP-dally* inserted in *dally*^{KO} rescued pMad defects (Fig. 3L-N, V) and adult wing defects of *dally*^{KO} mutants (Fig. 3P-R, W). In contrast, *3xHA-dlp* insertion into *dally*^{KO} failed to rescue pMad defects (Fig. 3M, O, V) or adult wing defects in *dally*^{KO} mutants (Fig. 3Q, S, W), although *3xHA-dlp* insertion into *dlp*^{KO} restored adult wing growth in *dlp*^{KO} mutants (Fig. 3T, U, W). Taken together, these results indicate that *dally*, but not *dlp*, is required for Dpp signaling gradient formation.

Interaction of the core protein of Dally with Dpp

How can only Dally be involved in Dpp signaling although both HSPGs are modified with HS chains (Fig. 2A, C)? Dally has been shown to interact with Dpp *in vitro* not only through the HS chains but also through the core protein [38]. Thus, we wondered whether the core protein of Dally can interact with Dpp in the wing disc to provide ligand specificity. To test this, we expressed *dally* or *dally*$^{\Delta HS}$, a *dally* mutant lacking all HS chain attachment sites [38] using *ap*-Gal4 to compare their ability to interact with Dpp and activate pMad signal. Upon *dally* expression in the dorsal compartment, HS chains, extracellular Dpp, and pMad signal increased as compared to the control, ventral compartment (Fig. 4A-C, G, J). In contrast, upon *dally*$^{\Delta HS}$ expression, HS chains rather decreased (Fig. 4D), probably because the core protein of Dally sequesters the factors required for synthesis of HS chains. Under this condition, extracellular Dpp still increased but pMad signal rather decreased (Fig. 4E, F, H, K). These results indicate that the core protein of Dally can interact with Dpp but this interaction is not sufficient but requires the HS chains to activate pMad signal.

Since Dally$^{\Delta HS}$ expression was higher than Dally expression (Fig. 4B', E'), we measured the relative Dpp accumulation against Dally or Dally$^{\Delta HS}$ expression (Fig. 4I) to address the relative contribution of the core protein and the HS chains for Dpp binding. We found that the relative Dpp accumulation upon *dally*$^{\Delta HS}$ expression is only slightly reduced compared to that upon *dally* expression (Fig. 4I), indicating a major contribution of the core protein in the interaction between Dally and Dpp in the wing disc.

HS chains of Dally are critical for Dpp distribution and signaling

The relatively minor contribution of HS chains of Dally for the interaction with Dpp raises questions on their requirement in Dpp distribution and signaling under physiological conditions. To address this, we inserted *YFP-dally*$^{\Delta HS}$, a *dally* mutant allele lacking HS chain modification [38], in the attP site of the *dally*^{KO} allele. We found that both pMad signaling (Fig. 4L-O) and extracellular Dpp distribution (Fig. 4P-S) were severely affected in the *YFP-dally*$^{\Delta HS}$ wing discs resembling the phenotypes of *dally*^{KO} mutants. Consistently, the *YFP-dally*$^{\Delta HS}$ adult wings mimicked patterning and growth defects of *dally*^{KO} adult wings (Fig. 4T-V). These results show that the interaction of the core protein of Dally with Dpp is not sufficient and that the HS chains of Dally are critical for Dpp distribution and signaling under physiological conditions.

HS chains of Dally control Dpp distribution and signaling largely independent of interaction with Dpp

How do HS chains of Dally control Dpp distribution and signaling gradient? The interaction of the HS chains of glypicans with Dpp is thought to be essential for their function. However, our data suggest that, while important for proper Dpp distribution and signaling, HS chains have only a very minor contribution to the binding of Dpp. To address whether a direct interaction of the HS chains of Dally and Dpp is critical, we sought to generate a Dpp variant that lacks HS-binding properties. A previous study showed that 7 basic amino acids at the N-terminus of the Dpp mature domain are crucial for the interaction with heparin but dispensable for interaction with receptors to activate downstream signaling [30]. To test the importance of this interaction *in vivo*, we generated *dpp$^{\Delta N}$*, a *dpp* mutant allele lacking the basic amino acid stretch. We found that the *dpp$^{\Delta N}$* allele is embryonic lethal, likely because the basic amino acids overlap with a collagen binding site and the Dpp-Collagen IV interaction is important for Dpp gradient formation in the early embryo [39]. To bypass this embryonic lethality without affecting wing disc development, we utilized a previously reported transgene called JAX, which contains the genomic region of *dpp* (JAX) critical for the early embryogenesis [40] but does not rescue the wing phenotypes of *dpp* mutants (Fig. S5). Indeed, the early lethality of homozygous *HA-dpp$^{\Delta N}$* was greatly rescued in the presence of this transgene (*JAX; HA-dpp$^{\Delta N}$*), thus allowing to investigate the requirement of the interaction of Dpp with the HS chains of Dally in later stages.

To test if Dpp$^{\Delta N}$ lacks interaction with Dally, we expressed *dally* or *dally$^{\Delta HS}$* in *JAX;dpp$^{\Delta N}$* using *ap*-Gal4 and compared their ability to interact with Dpp$^{\Delta N}$ (Fig. 5A, B). We found that, in both cases, extracellular distribution of Dpp$^{\Delta N}$ increased in the dorsal compartment (Fig. 5A, B), indicating that Dpp$^{\Delta N}$ can interact with the core protein of Dally. To address the relative contribution of the HS chains and the core protein for Dpp$^{\Delta N}$-Dally interaction, Dpp$^{\Delta N}$ accumulation was normalized against Dally or Dally$^{\Delta HS}$ expression since Dally$^{\Delta HS}$ expression was higher than Dally expression (Fig. 5A', B'). We found that the resulting normalized Dpp$^{\Delta N}$ accumulation was not changed between two conditions (Fig. 5C), indicating that the observed Dpp$^{\Delta N}$ accumulation upon Dally expression is through Dally-core protein and Dpp$^{\Delta N}$ indeed lacks interaction with HS.

Using the same experimental setup, we then compared the ability of Dally and Dally$^{\Delta HS}$ to activate Dpp signal in *JAX;dpp$^{\Delta N}$* (Fig.5A", B"), in which HS chains-Dpp interaction is lost (Fig. 5C). We found that Dally expression (Fig. 5A", D), but not Dally$^{\Delta HS}$ expression (Fig. 5B", E), expanded Dpp signaling in *JAX;dpp$^{\Delta N}$*, indicating that Dally can activate Dpp signaling through HS chains but independent of HS chains-Dpp interaction.

Surprisingly, and in contrast to *dally^{KO}* or *dally$^{\Delta HS}$* flies (Fig. 3, 4), we found that *JAX; HA-dpp$^{\Delta N}$* allele showed very subtle defects in Dpp distribution and signaling in wing discs (Fig. 5F-I) and in patterning and growth in adult wings (Fig. 5J-L). Indeed, while *dally^{KO}* and *dally$^{\Delta HS}$* adult wings are 25-30% smaller than control wings (Fig. 3J, W, 4V), *JAX; HA-dpp$^{\Delta N}$* adult wings are only 6.4% smaller than control wings (Fig.5L). Taken together, these results suggest that, although the HS chains of Dally are essential for Dpp distribution and signaling (Fig. 4), a direct interaction of HS chains of Dally with Dpp is largely dispensable (Fig. 5).

HS chains of Dally stabilize Dpp by antagonizing Tkv-mediated Dpp internalization

So far, all the models on how glypicans control Dpp distribution and signaling are based on direct interaction of the HS chains with Dpp (Fig. 1). How can the HS chains of Dally control Dpp distribution and signaling without directly interacting with Dpp? Among the models, we wondered whether Tkv is a factor through which HS chains of Dally can act (Fig 1D), although HS chains are thought to act through Dpp in the original model [30].

We first revisited the role of Tkv. According to the model [30] (Fig. 1D), Tkv is the Dpp receptor on the cell surface that internalizes and degrades Dpp in addition to activating pMad signal and Dally antagonizes internalization of Dpp to control extracellular Dpp distribution. In contrast, a recent study proposed that Dally, but not Tkv, internalizes Dpp [25]. To address this discrepancy, we first depleted *tkv* by RNAi using *ap*-Gal4 and visualized endogenous extracellular Dpp distribution. If Tkv is required for Dpp internalization, extracellular Dpp distribution should increase by removing Tkv. Indeed, we found that extracellular Dpp increased and expanded in the dorsal compartment (Fig. 6A, C), indicating that Tkv is required to internalize Dpp.

To address whether Dally antagonizes Tkv-mediated Dpp internalization, we asked if the defects in Dpp distribution in *dally* mutants can be rescued by RNAi-mediated depletion of *tkv*. We found that the extracellular Dpp gradient was expanded in the dorsal compartment (Fig. 6B, D), indicating that Dally

antagonizes Tkv-mediated Dpp internalization. Expanded Dpp distribution in *dally* mutants upon blocking Dpp internalization also suggests that Dally is largely dispensable for Dpp spreading, and that there are factors other than Tkv and Dally that bind to Dpp on the cell surface.

We then tested if Dally can promote Dpp internalization independent of antagonizing Tkv-mediated Dpp internalization. In this scenario, extracellular Dpp distribution should increase in *dally* mutants in the absence of *tkv*. To test this, we compared extracellular Dpp levels in the dorsal compartment of *ap>tkv RNAi* wing discs (Fig. 6A) and that of *ap>tkv RNAi, dally*^{KO} wing discs (Fig. 6B). We found that extracellular Dpp levels do not further increase (Fig. 6E), indicating that Dally is not essential to internalize Dpp.

Interestingly, when *tkv* was depleted in the dorsal compartment, pMad was not only lost from the dorsal compartment but also upregulated in ventral cells along the dorsal-ventral compartment boundary (arrow, Fig. 6F). This observation is consistent with the idea that, upon blocking internalization, Dpp from the dorsal compartment can reach to the ventral compartment to activate pMad through Tkv binding. In contrast, this phenotype was not seen upon depletion of *dally* by RNAi, although depletion of *dally* in the dorsal compartment mimicked the pMad defects of *dally* mutants (Fig 6G).

While HS chains of Dally are thought to compete with Tkv for binding to Dpp in the original model [30] (Fig. 1D), the minor phenotypes of *dpp*$^{\Delta N}$ (Fig. 4, 5) suggest that HS chains act through a different mechanism. To test if the HS chains of Dally stabilizes Dpp on the cell surface by antagonizing Tkv-mediated Dpp internalization, we depleted *tkv* by RNAi using *ap*-Gal4 in *dally*$^{\Delta HS}$ mutants. We found that extracellular Dpp gradient expanded in the dorsal compartment (Fig. 6H, I), thus indicating that the HS chains of Dally antagonize Dpp internalization.

Cumulatively, these results suggest that Tkv, but not Dally, is essential to internalize Dpp, and support a model, in which HS chains of Dally stabilizes Dpp on the cell surface by blocking Tkv-mediated Dpp internalization [30].

Discussion

HSPGs are essential for Dpp/BMP morphogen gradient formation and signaling in the Drosophila wing disc. Although a variety of models have been proposed, it remains largely unknown how distinct HSPGs control Dpp gradient formation and signaling. In this study, we generated and utilized genome engineering platforms for two HSPGs, *dally* and *dlp*, and *dpp* [15] to address this question.

Mechanism of Dally function

It has been thought that Dally and Dlp act redundantly to control Dpp signaling. However, we demonstrate here that Dally, but not Dlp, is critical for Dpp distribution and signaling through interaction of the core protein of Dally with Dpp (Fig. 2-4). We do not know if the interaction is direct but previous surface plasmon resonance (SPR) and co-immunoprecipitation experiments suggest that this is the case [38]. It has recently been shown that a specific structure, present in the core protein of Dlp but absent in Dally, shields the lipid moiety of Wg and is important for its spreading [41]. Thus, each glypican appears to acquire ligand specificity through its core protein.

In contrast to Wg, Dpp has no lipid modification and is diffusible by nature. Indeed, the expanded Dpp distribution in *dally* mutants upon blocking Dpp internalization (Fig. 6) does not support the idea that Dally is required for Dpp spreading itself [23,34,42] (Fig. 1B) or that Dally and Tkv are essential for blocking Dpp leakage from the wing epithelia [34]. This result suggests that there are other cell surface molecules that bind to Dpp on the cell surface. It remains to be tested if Dpp spreads by free diffusion or requires such factors. It is also unlikely that Dally inhibits Dpp spreading (Fig. 1C), since extracellular Dpp distribution expanded upon *dally* expression (Fig. 2) and Dpp distribution did not expand in *dally* mutants when Tkv-meidated Dpp internalization was blocked (Fig. 6E). Our results thus indicate that Dally acts downstream of Dpp spreading.

Despite the interaction of the core protein of Dally with Dpp upon Dally overexpression, this interaction is not sufficient to control Dpp distribution and Dpp signaling at its physiological level, and HS chains of Dally are absolutely essential for both processes (Fig. 4). Since increase of HS chains was not sufficient for interaction with Dpp (Fig. 2C, D), we speculate that HS chains of Dally act downstream of the interaction of the core protein of Dally with Dpp.

Among the proposed models (Fig. 1), our results support a model, in which Dally stabilizes Dpp on the cell surface by antagonizing Tkv-mediated internalization of Dpp [30] (Fig. 1D, 7A). Consistently, pulse-chase experiments showed that Dpp is less stable in *dally* mutants [30]. However, while the original model indicates that HS chains compete with Tkv for Dpp binding [30] (Fig.1D, 7A), our results suggest that HS chains act largely through Tkv based on two observations (Fig. 7B). First, although the *dally*$^{\Delta HS}$ allele showed severe defects similar to the *dally*^{KO} allele, the defects of the *dpp*$^{\Delta N}$ allele were surprisingly mild despite the lack of interaction with HS chains (Fig. 4, 5), indicating that HS chains act largely through other molecules. Second, defects in Dpp distribution in *dally*$^{\Delta HS}$ were rescued by removing *tkv* (Fig. 6). These results indicate that HS chains act through Tkv, rather than through Dpp, to stabilize Dpp on the cell surface (Fig. 7C-E).

It remains unknown how HS chains of Dally stabilize Dpp through Tkv. Since heparin has been shown to bind to BMP receptors [43], the HS chains of Dally may directly interact with Tkv to stabilize Dpp on the cell surface. Interestingly, we found that the HS chains of Dally control Dpp signaling also largely independent of interaction with Dpp (Fig. 5D, E), which likely reflects the role of Dally as a co-receptor. The simplest possibility is that the HS chains of Dally control both Dpp stability and signaling through Tkv (Fig. 7), but it is equally possible that the HS chains of Dally control Dpp signaling through other factors. In the future, it will be also important to address how the interaction of the core protein of Dally with Dpp and functions of HS chains through Tkv are coordinated.

Mechanisms of Dpp internalization

Our proposed model is based on the result that Dpp is internalized by Tkv (Fig. 6), consistent with a widely accepted idea that extracellular morphogens are removed by their receptors. However, this result contradicts a recent report proposing that Dally, but not Tkv, internalizes and recycles Dpp [25]. How can we explain the discrepancy?

If Tkv is involved in internalization of Dpp, internalized Dpp should decrease upon loss of *tkv*. Romanova-Michaelides et al. applied a nanobody internalization assay to visualize internalized Dpp [25]. In this assay, extracellular GFP-Dpp was first labeled using fluorophore conjugated anti-GFP nanobodies under endocytosis-restricted condition. After allowing internalization of the labelled GFP-Dpp, extracellular anti-GFP nanobodies were then stripped away by acid wash to follow only the internalized Dpp. Using this assay, Romanova-Michaelides et al. surprisingly found that internalization of GFP-Dpp was not affected in *tkv* mutant clones However, the experiment was performed under overexpression of GFP-Dpp from the anterior stripe of cells, in which the authors estimate 400 times higher expression than the physiological level. Under such unphysiological conditions, Dpp internalization through other Dpp binding factors can easily mask the impact of Tkv on Dpp internalization. Consistently, we found that Dpp binds to the cell surface without Tkv and Dally (Fig. 6).

If Tkv is involved in Dpp internalization, extracellular Dpp should increase upon loss of *tkv*. Romanova-Michaelides et al. used the observation that extracellular GFP-Dpp did not increase in *tkv* mutant clones upon GFP-Dpp expression from the anterior stripe of cells [42] to further support Tkv-independent Dpp internalization [25]. However, under 400 times higher expression levels of GFP-Dpp than the physiological level, it is not surprising that an increase of extracellular Dpp can be missed. Indeed, we find that endogenous extracellular Dpp is increased upon *tkv* depletion, indicating that Dpp is internalized through Tkv (Fig. 6). Notably, even when GFP-Dpp was overexpressed, accumulation of GFP-Dpp on the surfaces of cells lacking Tkv have been previously reported [44].

Romanova-Michaelides et al. proposed that, instead of Tkv, Dally is required for internalization of Dpp based on reduced internalization of endogenous GFP-Dpp upon blocking HS chain synthesis or upon cleaving HSPGs using the nanobody internalization assay [25]. In contrast, our results suggest that Dally rather antagonizes internalization of Dpp by blocking Tkv-mediated internalization of Dpp (Fig. 6). How can Dpp internalization be reduced in *dally* mutants if Dally antagonizes internalization of Dpp? We found that extracellular Dpp distribution is severely reduced in *dally* mutants due to Tkv-mediated internalization of Dpp (Fig. 6), indicating that the amount of extracellular Dpp available for labeling with nanobody is reduced in *dally* mutants. Thus, we speculate that the reduced internalization of Dpp in *dally* mutants revealed by the nanobody internalization assay reflects the reduced extracellular Dpp rather than reduced ability to internalize Dpp.

Our results do not thus support Dally-mediated internalization and recycling of Dpp as a mechanism of Dpp gradient scaling [25], although recycling of Dpp through other factors may contribute to Dpp gradient scaling. It

387 would be interesting to test if the Dally-mediated Dpp stabilization on the cell surface is involved in the Dpp
388 gradient scaling. Consistent with this, decrease of Dpp degradation rates has previously been proposed as
389 a mechanism for Dpp gradient scaling [45]. Furthermore, previous pulse-chase experiments showed that,
390 similar to Dally, Pentagone (Pent), a secreted feedback factor required for Dpp gradient scaling, is required
391 for Dpp stability [46]. Interestingly, Pent has been shown to interact with HS chains of Dally [46] [47], raising a
392 possibility that interaction of HS chains of Dally with Pent is critical for Dpp stability, thereby Dpp gradient
393 scaling.
394
395 **Conclusion**
396 To recognize and activate the specific signal, the affinity of a morphogen to its receptors is high. However,
397 the high affinity of the morphogen-receptor interaction could at the same time compromise the range of
398 morphogens through receptor-mediated removal of morphogens from the extracellular space. Thus, there
399 must exist mechanisms ensuring long-range action of the morphogen despite its high receptor affinity. Our
400 results suggest that Dally counteracts the internalization of Dpp through Tkv to increase the chance that Dpp
401 can reach further despite the high affinity of Dpp to Tkv.
402

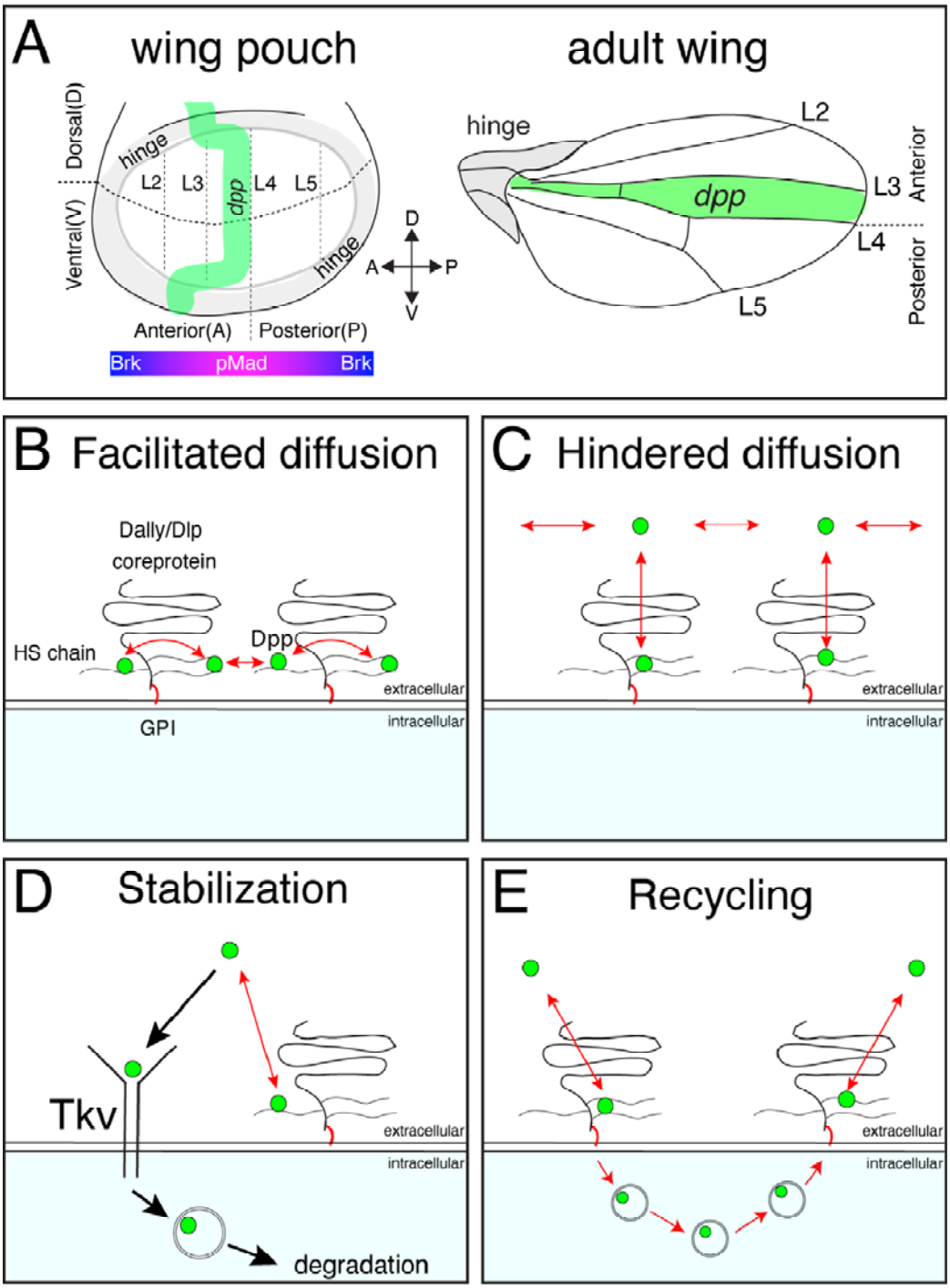

Fig.1 Distinct models on the roles of HSPGs on Dpp/BMP gradient formation
(**A**) Schematic view of the wing pouch (future wing tissue) and adult wing tissue. Dpp spreads from the anterior stripe of cells along the A-P compartment boundary to generate pMad gradient and an inverse Brk gradient to specify adult wing veins such as L2 and L5. (**B**) HSPGs are proposed to transport Dpp via repetitive interaction of HS chains with Dpp (facilitated diffusion model.) (**C**) HSPGs are proposed to hinder Dpp spreading via reversible interaction of HS chains with Dpp (Hindered diffusion model). (**D**) HSPGs are proposed to stabilize Dpp on the cell surface via reversible interaction of HS chains with Dpp that antagonizes Tkv-mediated Dpp internalization. (**E**) HSPGs are proposed to internalize and recycle Dpp.

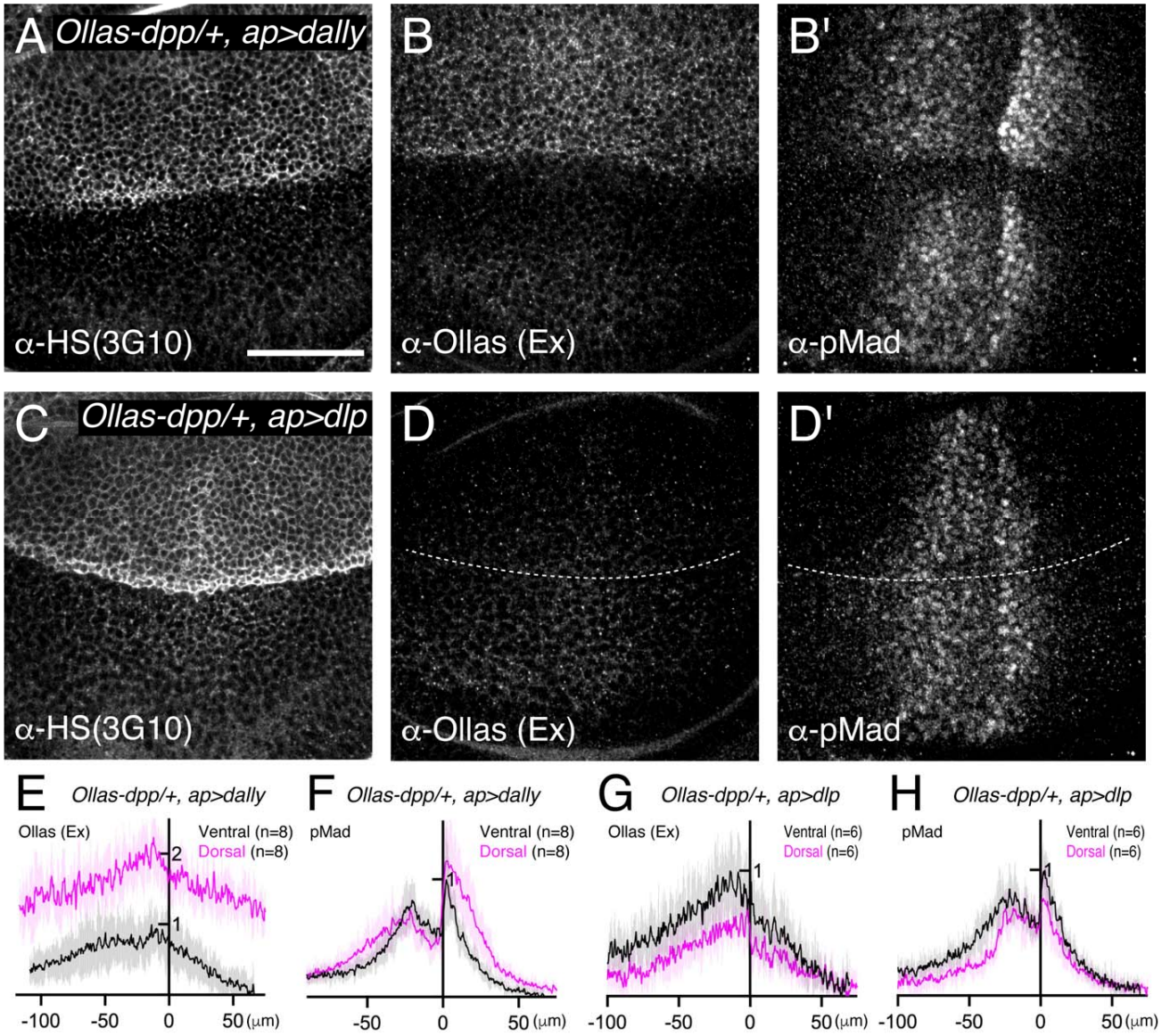

Fig. 2. Dally, but not Dlp, interacts with Dpp
(**A**-**D**) α-HS (3G10) (**A**, **C**), extracellular α-Ollas (**B**, **D**), and α-pMad (**B'**, **D'**) staining of *Ollas-dpp/+, ap>dally* disc (**A**-**B**) and *Ollas-dpp/+, ap>dlp* disc (**C**-**D**). (**E**-**H**) Average fluorescence intensity profile of (**B**, **B'**, **D**, **D'**) respectively. Data are presented as mean +/- SD. Scale bar: 50μm.

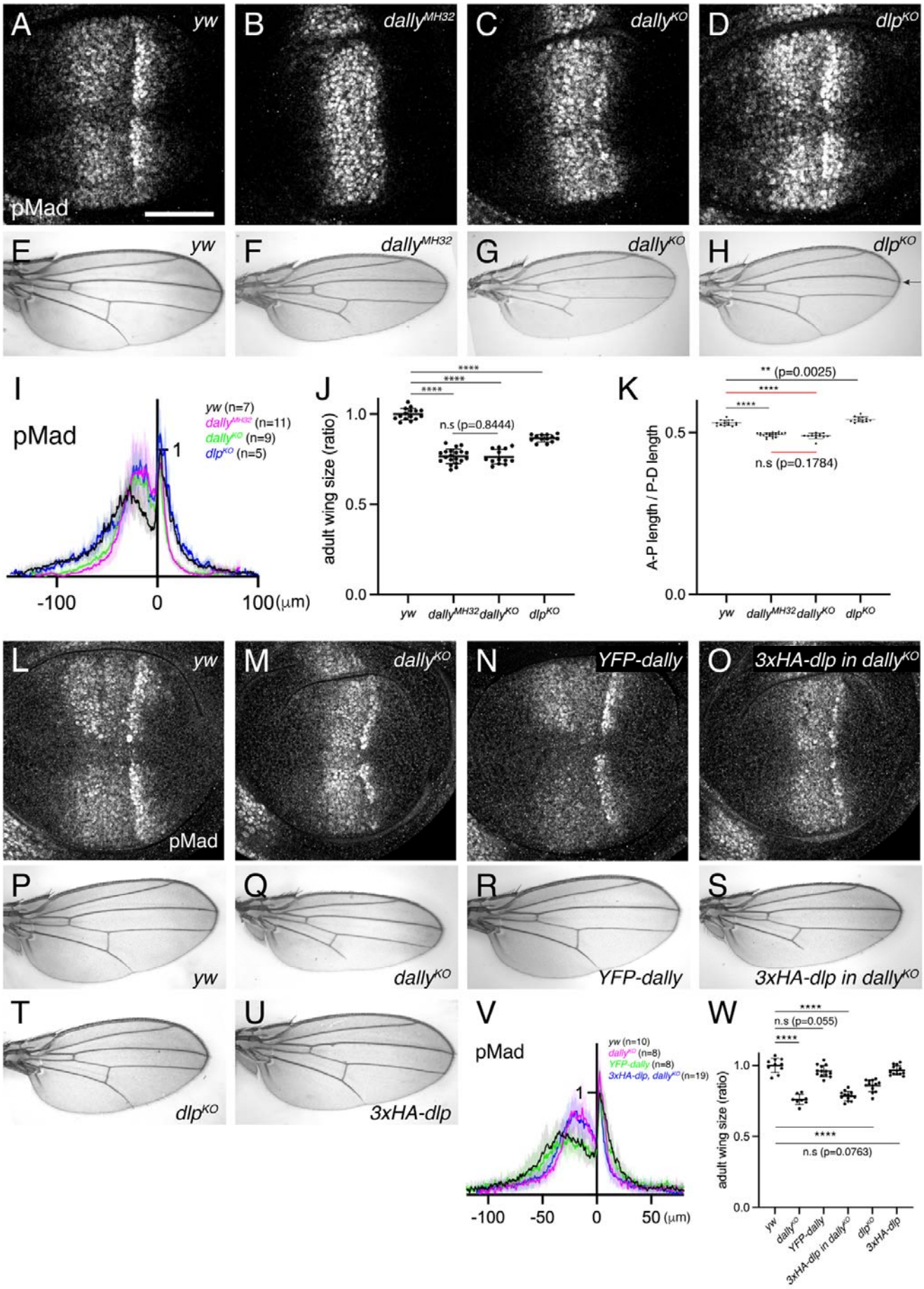
A
yw
pMad
B
dally^MH32
C
dally^KO
D
dlp^KO
E
yw
F
dally^MH32
G
dally^KO
H
dlp^KO
I
pMad
yw (n=7)
dally^MH32 (n=11)
dally^KO (n=9)
dlp^KO (n=5)
1
-100
0
100 (μm)
J
adult wing size (ratio)
1.0
0.5
0.0
****
****
****
n.s (p=0.8444)
yw
dally^MH32
dally^KO
dlp^KO
K
A-P length / P-D length
0.5
0.0
** (p=0.0025)
****
****
n.s (p=0.1784)
yw
dally^MH32
dally^KO
dlp^KO
L
yw
pMad
M
dally^KO
N
YFP-dally
O
3xHA-dlp in dally^KO
P
yw
Q
dally^KO
R
YFP-dally
S
3xHA-dlp in dally^KO
T
dlp^KO
U
3xHA-dlp
V
pMad
yw (n=10)
dally^KO (n=8)
YFP-dally (n=8)
3xHA-dlp, dally^KO (n=19)
1
-100
-50
0
50 (μm)
W
adult wing size (ratio)
1.0
0.5
0.0
****
n.s (p=0.055)
****
****
n.s (p=0.0763)
yw
dally^KO
YFP-dally
3xHA-dlp in dally^KO
dlp^KO
3xHA-dlp

425

Fig. 3. Dally, but not Dlp, is required for Dpp signaling gradient

(**A**-**D**) α-pMad staining of *yw* (**A**), *dally*^{MH32} (**B**), *dally*^{KO} (**C**), and *dlp*^{KO} (**D**) wing disc. (**E**-**H**) Adult wings of *yw* (**E**), *dally*^{MH32} (**F**), *dally*^{KO} (**G**), and *dlp*^{KO} (**H**). (**I**) Average fluorescence intensity profile of (**A**-**D**). Data are presented as mean +/- SD. (**J**) Comparison of adult wing size of *yw* (n=15), *dally*^{MH32} (n=20), *dally*^{KO} (n=13), and *dlp*^{KO} (n=13). Data are presented as mean +/- SD. Two-sided unpaired Student's t test with unequal variance was used for all the comparison. ****$p < 0.0001$. n.s; not significant. (**K**) Comparison of normalized A-P length against D-V length of adult wings of *yw* (n=15), *dally*^{MH32} (n=20), *dally*^{KO} (n=13), and *dlp*^{KO} (n=13). Data are presented as mean +/- SD. Two-sided unpaired Student's t test with unequal variance was used for comparison under black lines. Two-sided Mann−Whitney test was used for comparison under red lines. ****$p < 0.0001$, **$p < 0.01$. (**L**-**O**) α-pMad staining of *yw* (**L**), *dally*^{KO} (**M**), *YFP-dally* (**N**), and *3xHA-dlp* in *dally*^{KO} (**O**) wing disc. (**P**-**U**) Adult wings of *yw* (**P**), *dally*^{KO} (**Q**), *YFP-dally* (**R**), *3xHA-dlp in dally*^{KO} (**S**), *dlp*^{KO} (**T**), and *3xHA-dlp* (**U**). (**V**) Average fluorescence intensity profile of (**L**-**O**). Data are presented as mean +/- SD. (**W**) Comparison of adult wing size of *yw* (n=10), *dally*^{KO} (n=8), *YFP-dally* (n=13), *3xHA-dlp in dally*^{KO} (n=13), *dlp*^{KO} (n=13), and *3xHA-dlp* (n=13). Data are presented as mean +/- SD. Two-sided unpaired Student's t test with unequal variance was used for all the comparison. ****$p < 0.0001$. Scale bar: 50μm.

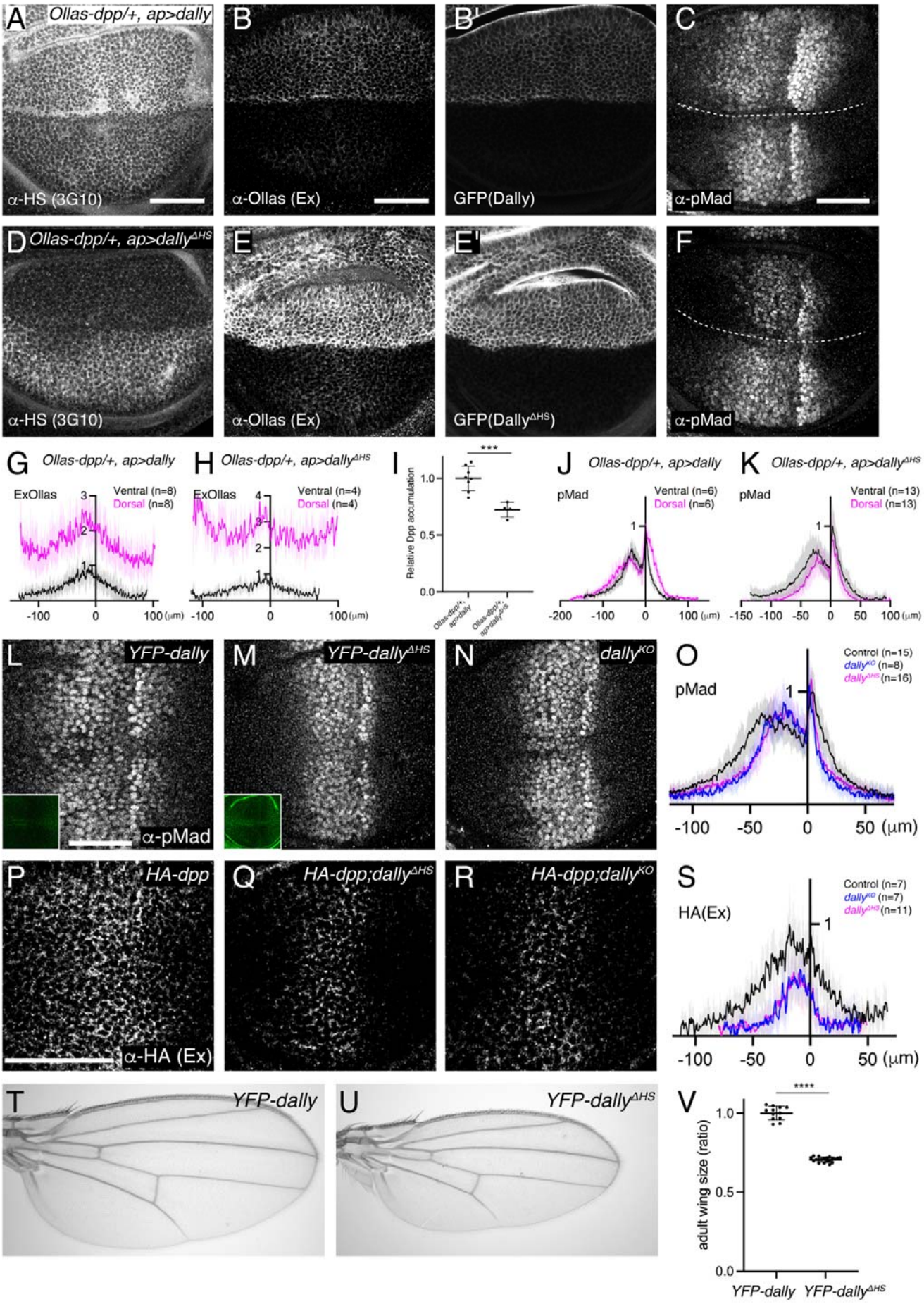
A Ollas-dpp/+, ap>dally
α-HS (3G10)
B
α-Ollas (Ex)
B'
GFP(Dally)
C
α-pMad
D Ollas-dpp/+, ap>dally^ΔHS
α-HS (3G10)
E
α-Ollas (Ex)
E'
GFP(Dally^ΔHS)
F
α-pMad
G Ollas-dpp/+, ap>dally
ExOllas
Ventral (n=8)
Dorsal (n=8)
H Ollas-dpp/+, ap>dally^ΔHS
ExOllas
Ventral (n=4)
Dorsal (n=4)
I
***
Relative Dpp accumulation
J Ollas-dpp/+, ap>dally
pMad
Ventral (n=6)
Dorsal (n=6)
K Ollas-dpp/+, ap>dally^ΔHS
pMad
Ventral (n=13)
Dorsal (n=13)
L YFP-dally
α-pMad
M YFP-dally^ΔHS
N dally^KO
O
pMad
Control (n=15)
dally^KO (n=8)
dally^ΔHS (n=16)
P HA-dpp
α-HA (Ex)
Q HA-dpp;dally^ΔHS
R HA-dpp;dally^KO
S
HA(Ex)
Control (n=7)
dally^KO (n=7)
dally^ΔHS (n=11)
T YFP-dally
U YFP-dally^ΔHS
V
****
adult wing size (ratio)
YFP-dally
YFP-dally^ΔHS

444
445

Fig.4. Interaction of core protein of Dally with Dpp

(**A**-**F**) α-HS (3G10) (**A**, **D**), extracellular α-Ollas (**B**, **E**), GFP (**B'**, **E'**), α-pMad (**C**, **F**) staining of *Ollas-dpp/+, ap>dally* disc (**A**-**C**) and *Ollas-dpp/+, ap>dally*$^{\Delta HS}$ disc (**D**-**F**). (**G**) Average fluorescence intensity profile of (**B**). (**H**) Average fluorescence intensity profile of (**E**). (**I**) Relative Dpp accumulation (α-Ollas signal) (**B**, **E**) normalized against expression level of Dally or Dally$^{\Delta HS}$ (GFP fluorescent signal) around the Dpp producing cells (**B'**, **E'**). Two-sided unpaired Student's t test with unequal variance was used for the comparison. ***$p < 0.001$. (**J**) Average fluorescence intensity profile of (**C**). (**K**) Average fluorescence intensity profile of (**F**). (**G**-**K**) Data are presented as mean +/- SD. (**L**-**N**) α-pMad staining of *YFP-dally* (**L**), *YFP-dally*$^{\Delta HS}$ (**M**), and *dally*^{KO} (**N**) wing disc. YFP signal of *YFP-dally* (**L, inset**) and *YFP-dally*$^{\Delta HS}$ (**M, inset**) wing disc. We note that, similar to the overexpression results (Fig. 4B', E'), *YFP-dally*$^{\Delta HS}$ wing discs showed higher expression levels than *YFP-dally*$^{\Delta HS}$ (Fig. 4L, M inset). (**O**) Average fluorescence intensity profile of (**L**-**N**). Data are presented as mean +/- SD. (**P**-**R**) Extracellular α-HA staining of *HA-dpp* (**P**), *HA-dpp; YFP-dally*$^{\Delta HS}$ (**Q**), and *HA-dpp; dally*^{KO} (**R**) wing disc. (**S**) Average fluorescence intensity profile of (**P**-**R**). Data are presented as mean +/- SD. (**T**-**U**) Adult wings of *YFP-dally* (**T**) and *YFP-dally*$^{\Delta HS}$ (**U**). (**V**) Comparison of adult wing size of *YFP-dally* (n=12) and *YFP-dally*$^{\Delta HS}$ (n=20). Data are presented as mean +/- SD. Two-sided unpaired Student's t test with unequal variance was used for the comparison. ****$p < 0.0001$. Scale bar: 50μm.

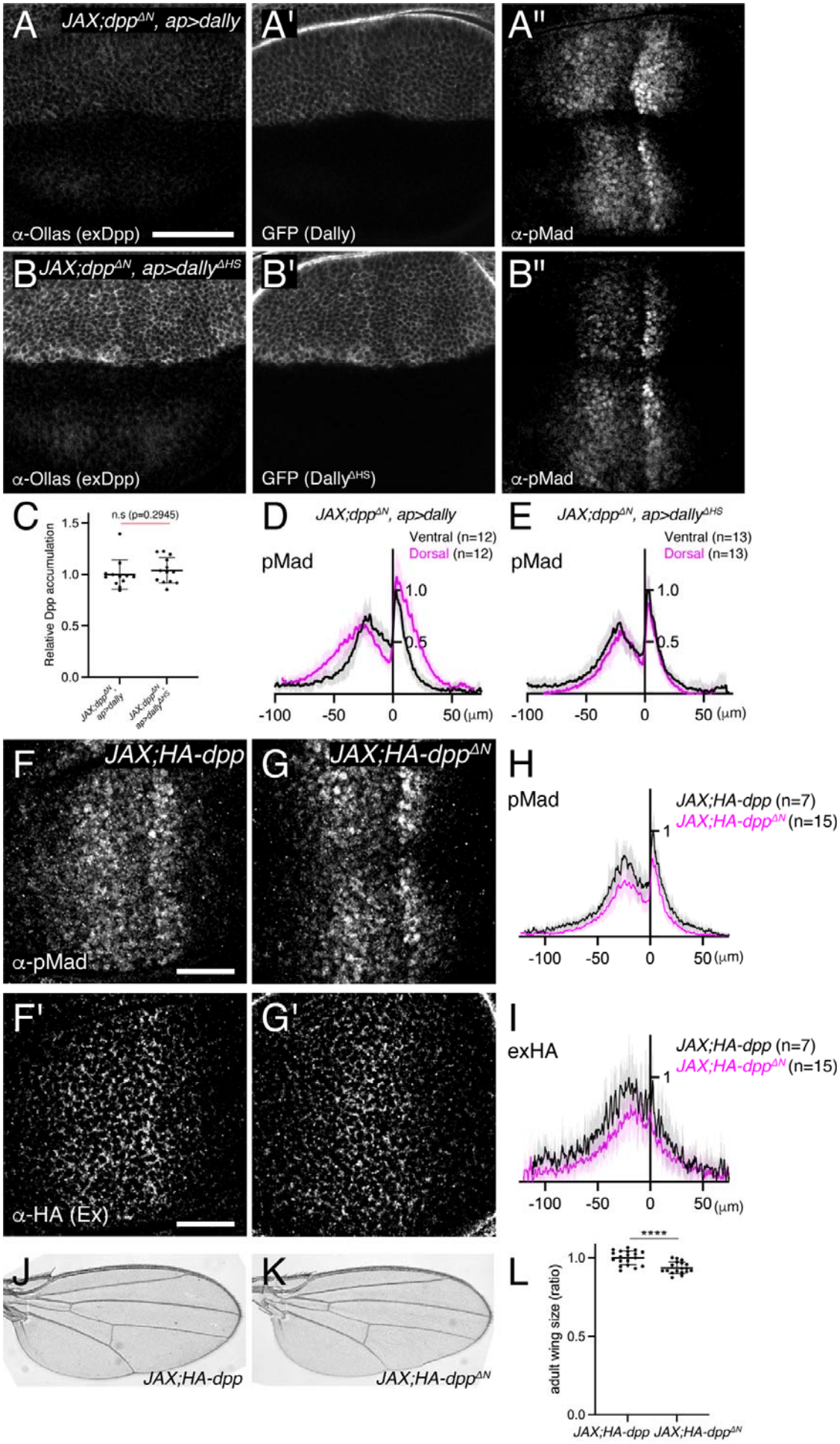
A
JAX;dpp^ΔN, ap>dally
α-Ollas (exDpp)
A'
GFP (Dally)
A''
α-pMad
B
JAX;dpp^ΔN, ap>dally^ΔHS
α-Ollas (exDpp)
B'
GFP (Dally^ΔHS)
B''
α-pMad
C
n.s (p=0.2945)
Relative Dpp accumulation
1.5
1.0
0.5
0.0
JAX;dpp^ΔN ap>dally
JAX;dpp^ΔN ap>dally^ΔHS
D
JAX;dpp^ΔN, ap>dally
Ventral (n=12)
Dorsal (n=12)
pMad
1.0
0.5
-100
-50
0
50 (μm)
E
JAX;dpp^ΔN, ap>dally^ΔHS
Ventral (n=13)
Dorsal (n=13)
pMad
1.0
0.5
-100
-50
0
50 (μm)
F
JAX;HA-dpp
α-pMad
G
JAX;HA-dpp^ΔN
H
pMad
JAX;HA-dpp (n=7)
JAX;HA-dpp^ΔN (n=15)
1
-100
-50
0
50 (μm)
F'
α-HA (Ex)
G'
I
exHA
JAX;HA-dpp (n=7)
JAX;HA-dpp^ΔN (n=15)
1
-100
-50
0
50 (μm)
J
JAX;HA-dpp
K
JAX;HA-dpp^ΔN
L
****
adult wing size (ratio)
1.0
0.5
0.0
JAX;HA-dpp
JAX;HA-dpp^ΔN

Fig. 5 HS chains of Dally act largely independent of interaction with Dpp

(**A**-**B**) extracellular α-Ollas (**A**, **B**), GFP (**A'**, **B'**), and α-pMad (**A''**, **B''**) staining of *JAX;HA-dpp$^{\Delta N}$, ap>dally* disc (**A-A''**) and *JAX;HA-dpp$^{\Delta N}$, ap>dally$^{\Delta HS}$* disc (**B-B''**). (**C**) Relative Dpp accumulation (α-Ollas signal) (**A**, **B**) normalized against expression level of Dally or Dally$^{\Delta HS}$ (GFP fluorescent signal) around the Dpp producing cells (**A'**, **B'**). Two-sided Mann−Whitney test was used for comparison. n.s; not significant. (**D**) Average fluorescence intensity profile of (**A''**). Data are presented as mean +/- SD. (**E**) Average fluorescence intensity profile of (**B''**). Data are presented as mean +/- SD. (**F**-**G**) α-pMad (**F**, **G**) and extracellular α-HA (**F'**, **G'**) staining of *JAX;HA-dpp* disc (**F**, **F'**) and *JAX;HA-dpp$^{\Delta N}$* disc (**G**, **G'**). (**H**) Average fluorescence intensity profile of (**F**, **G**). Data are presented as mean +/- SD. (**I**) Average fluorescence intensity profile of (**F'**, **G'**). Data are presented as mean +/- SD. (**J**-**K**) Adult wings of *JAX;HA-dpp* (**J**) and *JAX;HA-dpp$^{\Delta N}$* (**K**). (**L**) Comparison of adult wing size of *JAX;HA-dpp* (n=19) and *JAX;HA-dpp$^{\Delta N}$* (n=18). Data are presented as mean +/- SD. Two-sided unpaired Student's t test with unequal variance was used for the comparison. ****$p < 0.0001$.

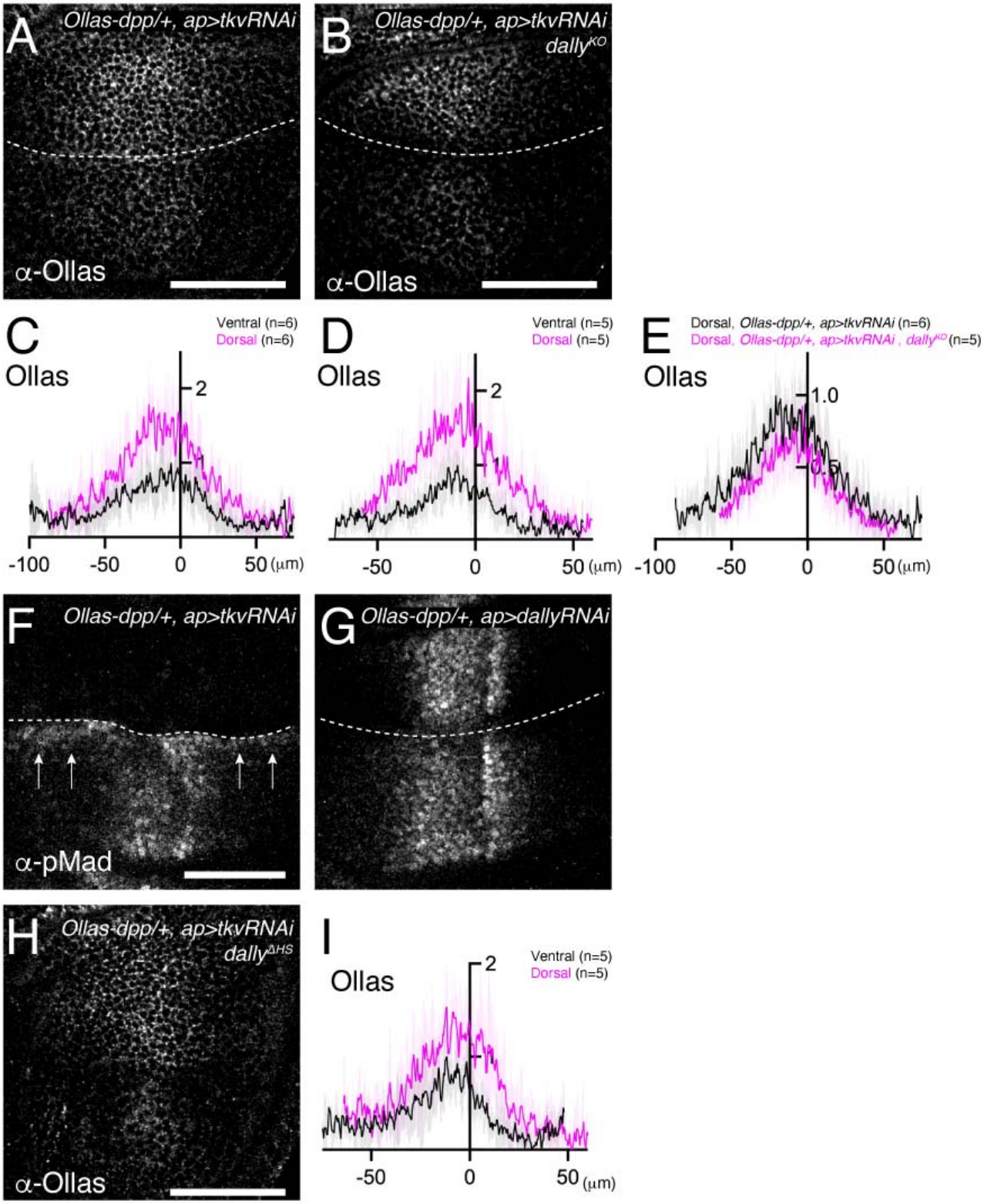
A
Ollas-dpp/+, ap>tkvRNAi
α-Ollas
B
Ollas-dpp/+, ap>tkvRNAi
dally^KO
α-Ollas
C
Ventral (n=6)
Dorsal (n=6)
Ollas
2
-100
-50
0
50 (μm)
D
Ventral (n=5)
Dorsal (n=5)
Ollas
2
-50
0
50 (μm)
E
Dorsal, Ollas-dpp/+, ap>tkvRNAi (n=6)
Dorsal, Ollas-dpp/+, ap>tkvRNAi , dally^KO (n=5)
Ollas
1.0
0.5
-100
-50
0
50 (μm)
F
Ollas-dpp/+, ap>tkvRNAi
α-pMad
G
Ollas-dpp/+, ap>dallyRNAi
H
Ollas-dpp/+, ap>tkvRNAi
dally^ΔHS
α-Ollas
I
Ventral (n=5)
Dorsal (n=5)
Ollas
2
-50
0
50 (μm)

478
479

480 **Fig. 6 HS chains of Dally stabilize Dpp by antagonizing Tkv-mediated Dpp internalization**
481 (**A, B**) Extracellular α-Ollas staining of *Ollas-dpp/+, ap>tkv RNAi* wing disc (**A**) and *dally*^{KO}, *Ollas-dpp/+,*
482 *ap>tkv RNAi* wing disc (**B**). (**C, D**) Average fluorescence intensity profile of (**A, B**) respectively. Data are
483 presented as mean +/- SD. (**E**) Average fluorescence intensity profile of the dorsal compartment of (**A**, **B**).
484 Data are presented as mean +/- SD. (**F**, **G**) α-pMad staining of *Ollas-dpp/+, ap>tkv RNAi* wing disc (**F**), and
485 *Ollas-dpp/+, ap>dally RNAi* wing disc (**G**). (**H**) Extracellular α-Ollas staining of *dally*$^{\Delta HS}$*, Ollas-dpp/+, ap>tkv*
486 *RNAi* wing disc. (**I**) Average fluorescence intensity profile of (**H**). Data are presented as mean +/- SD. Scale
487 bar: 50μm.
488

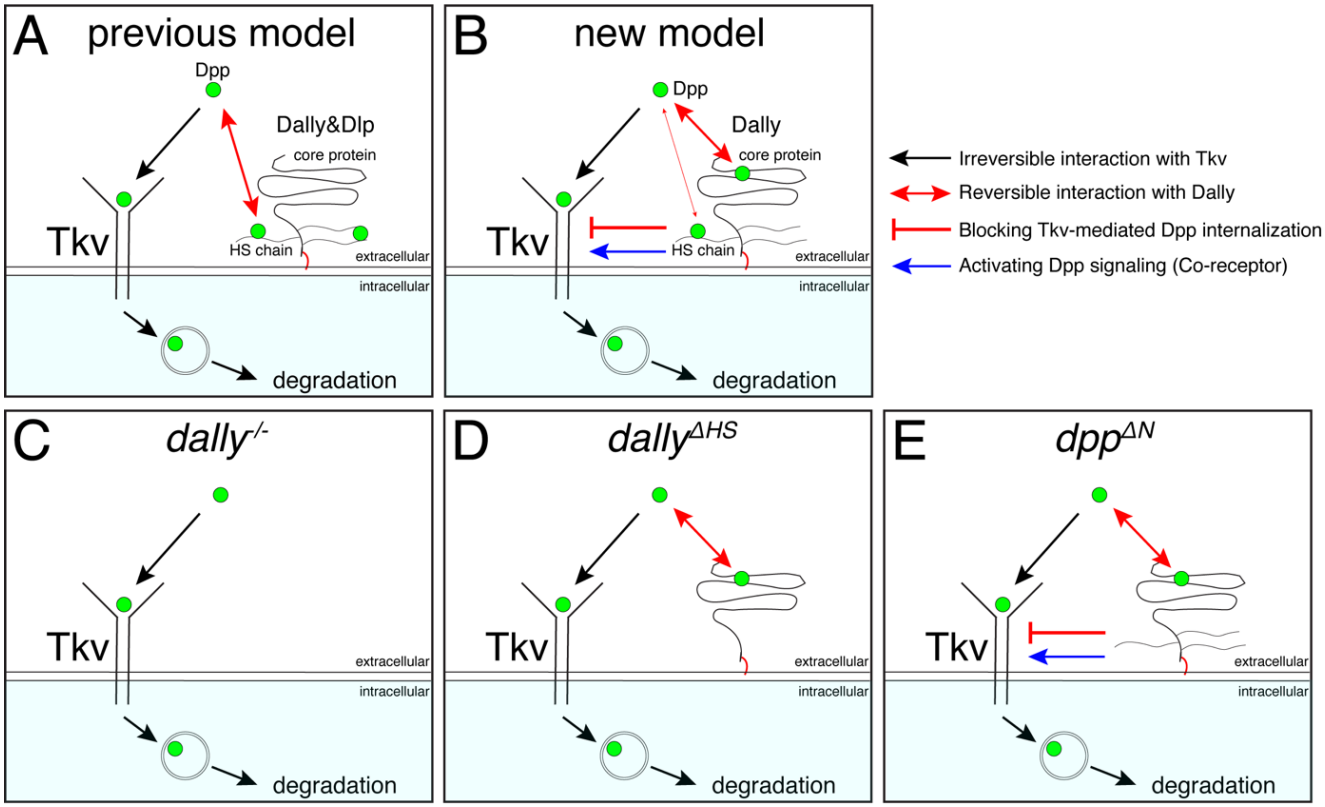

Fig. 7 A revised model on the roles of Dally on Dpp/BMP gradient formation and signaling
(**A**) A previous model. Dally and Dlp competes with Tkv for Dpp binding to antagonize Tkv-mediated Dpp internalization. (**B**) A revised model. Dally, but not Dlp, reversibly interacts with Dpp partially through its HS chains and mainly through its core protein. The former interaction is not essential and the latter interaction is not sufficient to antagonize Tkv-mediated Dpp internalization under physiological conditions. Upon interaction of Dpp with the core protein of Dally, HS chains of Dally antagonize Tkv-mediated Dpp internalization through Tkv to stabilize Dpp on the cell surface. HS chains of Dally control Dpp signaling also independent of interaction with Dpp likely through Tkv. It remains unknown whether and how Dpp signal activation by core protein bound Dpp and stability by HS chains are coordinated. (**C**) In *dally*^{KO} mutants, Tkv-mediated Dpp internalization by Tkv is not antagonized. Dpp is irreversibly bound to Tkv and then removed by Tkv from the extracellular space and degraded. (**D**) In *dally*$^{\Delta HS}$ mutants, the core protein of Dally can interact with Dpp but this interaction is not sufficient to antagonize Tkv-mediated Dpp internalization. Without HS chains, Dpp is irreversibly bound to Tkv and then removed by Tkv from the extracellular space and degraded. (**E**) In *dpp*$^{\Delta N}$ mutants, Dpp can interact with core protein but not with HS chains of Dally. Without interaction of HS chains with Dpp, HS chains can antagonize Tkv-mediated Dpp internalization through Tkv to stabilize Dpp on the cell surface.

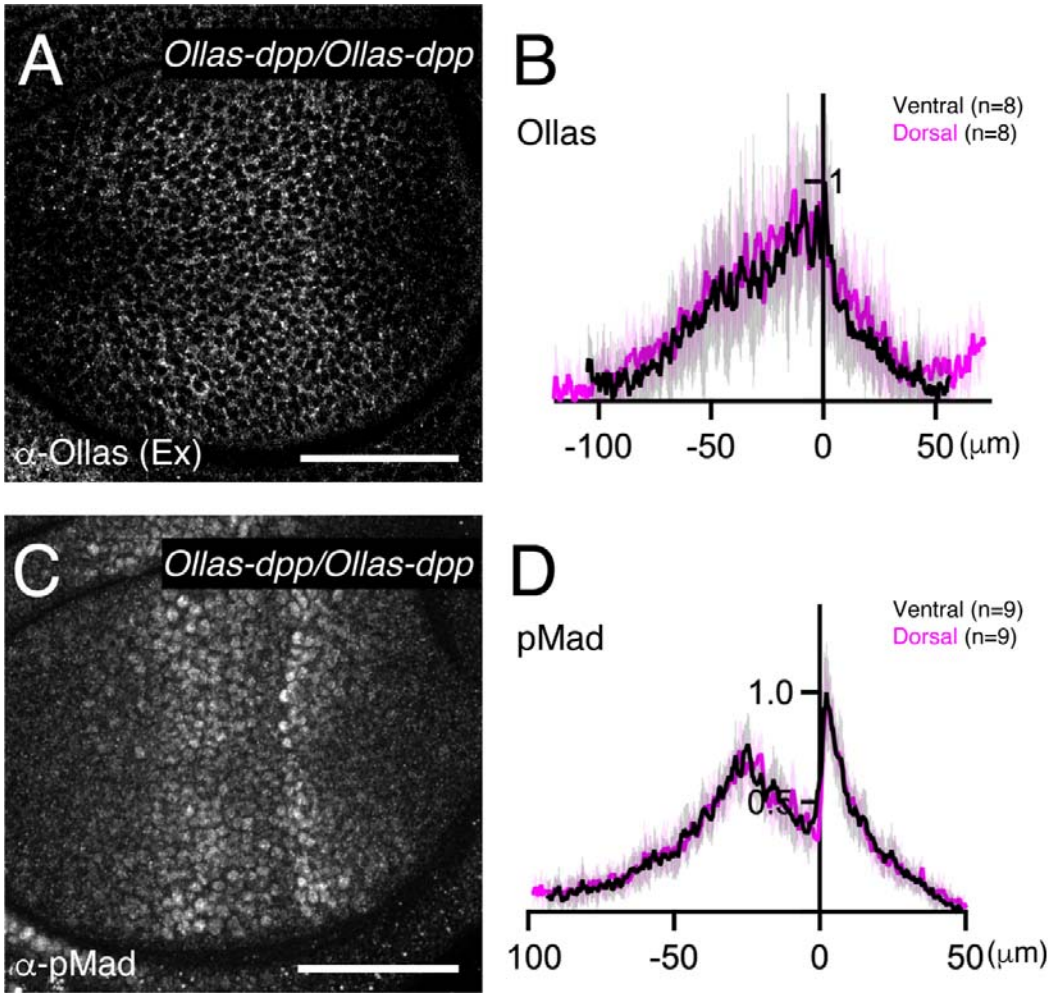

Fig. S1 Comparison of endogenous Dpp gradient and signaling between dorsal and ventral compartment

(**A**) Extracellular α-Ollas staining of *Ollas-dpp/Ollas-dpp* wing disc. (**B**) Average fluorescence intensity profile of (**A**). (**C**) α-pMad staining of *Ollas-dpp/Ollas-dpp* wing disc. (**D**) Average fluorescence intensity profile of (**C**).

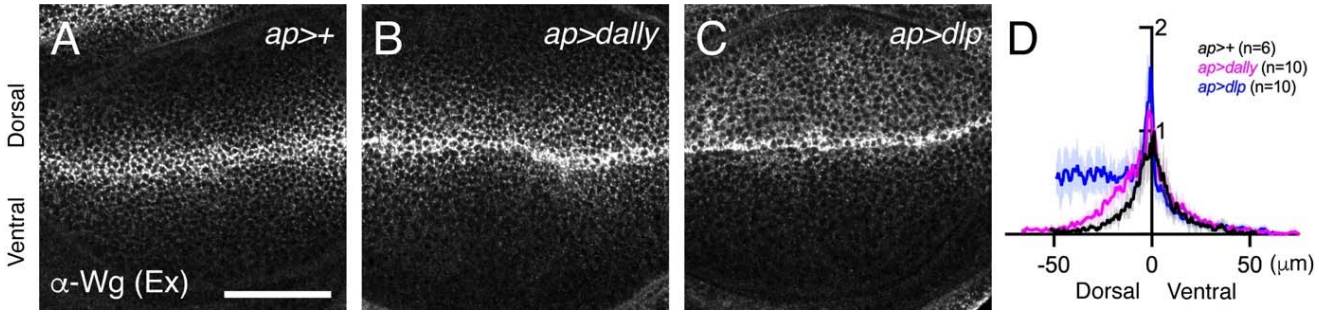

Fig. S2 Preferential interaction of Dlp with Wg

(**A**) Extracellular α-Wg staining of *Ollas-dpp/+* (**A**), *Ollas-dpp/+, ap>dally* (**B**), and *Ollas-dpp/+, ap>dlp* (**C**). (**D**) Average fluorescence intensity profile of (**A-C**).

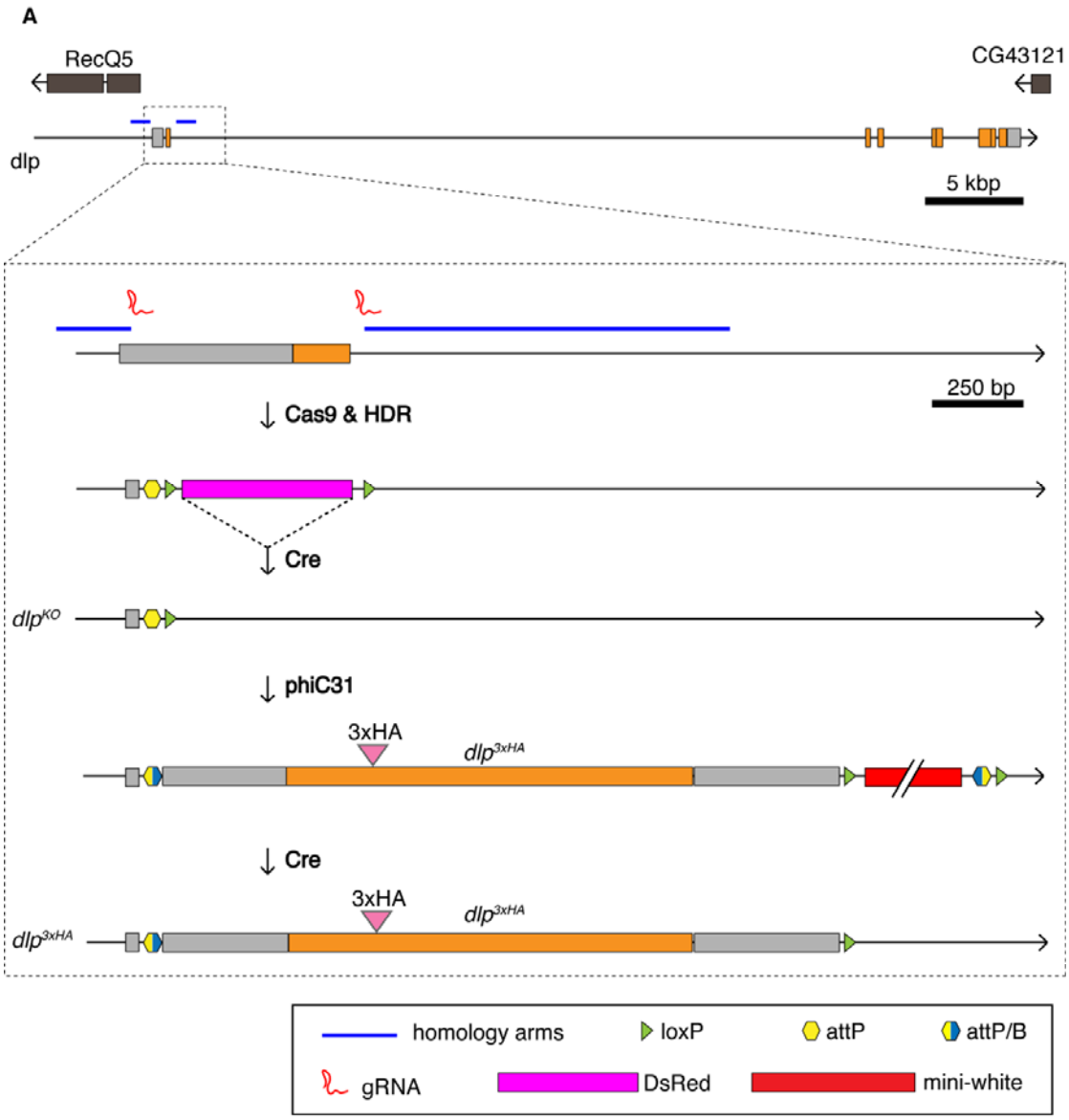

B

dally^{KO}

ATTTAGCCCCATCATCCACTGTGTCTGCACACAGAAATCACCCATCAAAACATATGCAGGTACCGTAGTGCCCCAACTG
GGGTAACCTTTGAGTTCTCTCAGTTGGGGGCGTAGTGTACCATAACTTCGTATAATGTATGCTATACGAAGTTATCACTA
GTGTAAAGTTCACGCCATCCATCCGTAGAGTTATAATATCGAGTATGCGCTT

dlp^{KO}

ATTGTTAATAATCCCGATTTAATAACACCCGACAACCATGCGGCCGCGGACATATGCACACCTGCGATCGTAGTGCCCC
AACTGGGGTAACCTTTGAGTTCTCTCAGTTGGGGGCGTAGATAACTTCGTATAATGTATGCTATACGAAGTTATAGAAG
AGCACTAGATGTCCGATATTATATACCAATGGCTTAATAAATACCTGTC

Fig. S3 Generation of *dally*^{KO} and *dlp*^{KO}

(**A**) Schematic view of manipulation of the glypican genomic loci exemplified with *dlp*. (**B**) the exact sequences at the lesion of *dally*^{KO} and *dlp*^{KO}: color code as in (**A**) (blue: genomic sequences at the inner boundaries of homology arms for HDR, yellow: attP, green: loxP, black: “scars” (remnants of vector sequences including cloning sites)**.**

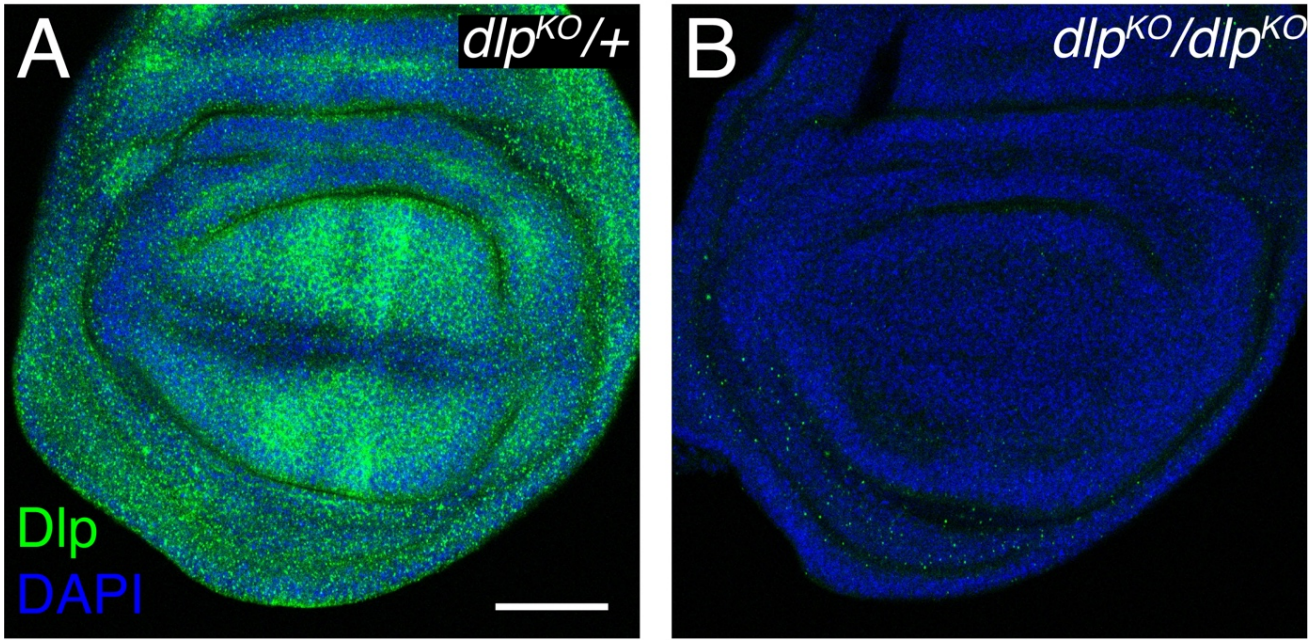

Fig. S4 Validation of *dlp^{KO}* allele
(**A, B**) α-Dlp and DAPI staining of *dlp^{KO}*/+ (**A**) and *dlp^{KO}*/ *dlp^{KO}* (**B**).

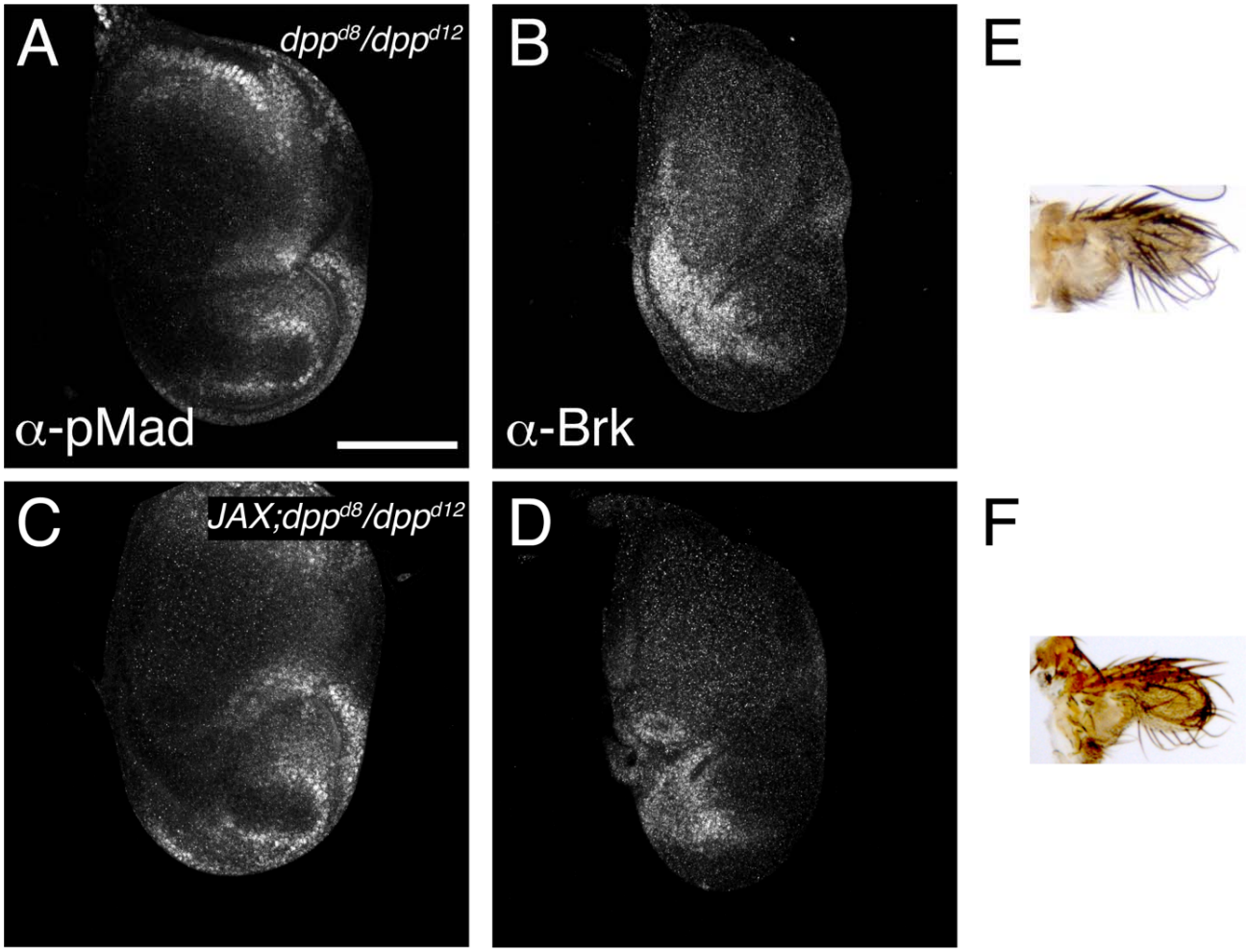

Fig. S5 *JAX* does not rescue *dpp* disc allele

(**A-D**) α-pMad staining (**A**, **C**) and α-Brk staining (**B**, **D**) of *dpp^{d8}/dpp^{d12}* (**A, B**) and *JAX;dpp^{d8}/dpp^{d12}* (**C, D**). (**E**, **F**) Adult wings of *dpp^{d8}/dpp^{d12}* (**E**) and *JAX;dpp^{d8}/dpp^{d12}* (**F**).

Materials and Methods

Data reporting

No statistical methods were used to predetermine sample size. The experiments were not randomized, and investigators were not blinded to allocation during experiments and outcome assessment.

Fly stocks

Flies for experiments were kept at 25°C in standard fly vials containing polenta and yeast. The following fly lines were used: *UAS-tkv-RNAi* (Bloomington 40937), *UAS-dally-RNAi* (VDRC 14136), *Ollas-dpp* [35], *UAS-GFP-HA-dally*, *UAS-GFP-dally*$^{\Delta HS}$ (Suzanne Eaton), *UAS-dlp* (Baeg et al., 2001), *HA-dpp* [15], *HA-dpp*$^{\Delta N}$ (this study), *dlp [ko;attB]* (this study), *dally[ko;attB]* (this study), *dally[YFP-dally;attP]* (this study), *dlp[3xHA-dlp;attP]* (this study) *dally[YFP-dally*$^{\Delta HS}$*;attP]* (this study), *dally[3xHA-dlp;attP]* (this study), *ap-Gal4* (Bloomington 3041), ap[c1.4b-Gal4] (Michèle Sickmann and Martin Müller, unpublished), *JAX* [40], *Ollas-HA-dpp*$^{\Delta N}$ (this study), *hh-Gal4* (Gift from Dr Manolo Calleja), *dally*^{MH32} [37]. *yw*, *dpp*^{d8} and *dpp*^{d12} are described from Flybase.

Genotypes by figures

Fig. 2A, B; *ap-Gal4, Ollas-dpp/+ ; UAS-GFP-HA-dally/+*
Fig. 2C, D; *ap-Gal4, Ollas-dpp/+ ; UAS-dlp/+*
Fig. 3A, E; *yw* (control)
Fig. 3B, F; *dally*^{MH32}*/dally*^{MH32}
Fig. 3C, G; *dally[KO;attB]/dally[KO;attB]*
Fig. 3D, H; *dlp[KO;attB]/dlp[KO;attB]*
Fig. 3L, P; *yw* (control)
Fig. 3M, Q; *dally[KO;attB]/dally[KO;attB]*
Fig. 3N, R; *dally[YFP-dally;attP]/dally[YFP-dally;attP]*
Fig. 3O, S; *dally[3xHA-dlp;attP]/dally[3xHA-dlp;attP]*
Fig. 3T; *dlp[KO;attB]/dlp[KO;attB]*
Fig. 3U; *dlp[3xHA-dlp;attP]/dlp[3xHA-dlp;attP]*
Fig.4A-C; *ap-Gal4, Ollas-dpp/+ ; UAS-GFP-HA-dally/+*
Fig.4D-F; *ap-Gal4, Ollas-dpp/+ ; UAS-GFP-dally*$^{\Delta HS}$
Fig.4L; *dally[YFP-dally;attP]/dally[YFP-dally;attP]*
Fig.4M; *dally[YFP-dallyΔHS;attP]/dally[YFP-dallyΔHS;attP]*
Fig.4N; *dally[KO;attB]/dally[KO;attB]*
Fig.4P; *HA-dpp/HA-dpp*
Fig.4Q; *HA-dpp/HA-dpp;dally[YFP-dallyΔHS;attP]w+/dally[YFP-dallyΔHS;attP]w+*
Fig.4R; *HA-dpp/HA-dpp;dally[KO;attB]/dally[KO;attB]*
Fig.4T; *dally[YFP-dally;attP]/dally[YFP-dally;attP]*
Fig.4U; *dally[YFP-dallyΔHS;attP]/dally[YFP-dallyΔHS;attP]*
Fig. 5A; *JAX; ap-Gal4, HA-dpp*$^{\Delta N}$*/ Ollas-HA-dpp*$^{\Delta N}$*;UAS-GFP-HA-dally/+*
Fig. 5B; *JAX; ap-Gal4, HA-dpp*$^{\Delta N}$*/ Ollas-HA-dpp*$^{\Delta N}$*;UAS-GFP-dally*$^{\Delta HS}$*/+*
Fig. 5F, J; *JAX;HA-dpp/HA-dpp*
Fig. 5G, K; *JAX;HA-dpp*$^{\Delta N}$*/HA-dpp*$^{\Delta N}$
Fig. 6A; *ap-Gal4, Ollas-dpp/UAS-tkvRNAi*
Fig. 6B; *ap-Gal4, Ollas-dpp/UAS-tkvRNAi;dally[KO;attB]/dally[KO;attB]*
Fig. 6F; *ap-Gal4, Ollas-dpp/UAS-tkvRNAi*
Fig. 6G; *ap-Gal4, Ollas-dpp/+; UAS-dallyRNAi/+*
Fig. 6H; *ap-Gal4, Ollas-dpp/UAS-tkvRNAi;dally[YFP-dallyΔHS;attP]w+/dally[YFP-dallyΔHS;attP]w+*

Fig. S1A, C; *Ollas-dpp/Ollas-dpp*
Fig. S2A; *ap-Gal4, Ollas-dpp/+*
Fig. S2B; *ap-Gal4, Ollas-dpp/+; UAS-GFP-HA-dally/+*
Fig. S2C; *ap-Gal4, Ollas-dpp/+; UAS-dlp/+*
Fig. S4A; *dlp[KO;attB]/+*
Fig. S4B; *dlp[KO;attB]/dlp[KO;attB]*
Fig. S5A, B, E; dpp^{d8}/dpp^{d12}
Fig. S5C, D, F; *JAX;* dpp^{d8}/dpp^{d12}

Generation of transgenic flies and alleles

HA-dpp$^{\Delta N}$ plasmid was constructed by GENEWIZ by removing 21bp encoding the 7 basic amino acids (RRPTRRK) from *HA-dpp* plasmid [15].

Ollas-HA-dpp$^{\Delta N}$ plasmid was constructed by using the *HA-dpp*$^{\Delta N}$ plasmid and the *Ollas-HA-dpp* plasmid as templates. Both plasmids were digested using XhoI and BspEI as restriction enzymes. The small fragment from the *HA-dpp*$^{\Delta N}$ plasmid and the large fragment from the *Ollas-HA-dpp* plasmid were used for ligation. Generation of endogenous *dpp* alleles using these plasmids were previously described [15].

Genomic manipulation of glypicans

The *dally*^{KO} and *dlp*^{KO} alleles were generated by replacing parts of the first exon of the genes with attP cassettes. In both cases, the deleted fragment comprise part of the 5' UTR, and the complete coding sequence, including the start codon and the signal peptide encoding sequence. For the generation of *dally*^{KO} homology arms flanking the target region were amplified by genomic PCR using primer pairs dally_5'_for (ATAGCTAGCCTCTAAAGACTCAAATTAATTAATTCATTTCAGATTGCGC) and dally_5'_rev (ATACATATGTTTTGATGGGTGATTTCTGTGTGCAGACACAGTG), or dally_3'_for (TATACTAGTGTAAAGTTCACGCCATCCATCCGTAGAGTTATAATATCG) and dally_3'_rev (ATAGGCGCGCCTTTCACTCAATTACACGAAACAGATATATATTGGGTACATTCGC) and cloned into the 5' MCS and 3' MCS of vector pTV(Cherry) using restriction enzymes NheI and NdeI or SpeI and AscI, respectively (restriction sites underlined). The construct was subjected to P-element transgenesis and was subsequently mobilized and linearized by crossing transgenic flies to flies carrying hsFLP and hsSceI and applying heat-shock as described [48].

The *dlp*^{KO} allele was generated by Cas9/CRISPR mediated homologous repair. Guide RNA sequences flanking the target region were GAAGCAATTGAAGTGCAACA and AATATCGGACATACCGTTAC and were cloned into plasmid pCFD3:U6:3. The two homology arms for homologous-directed repair were amplified by genomic PCR using primer pairs dlp_5'_for (TTTTCTCGAGCATGCTGGGCATCGACACATACACATCC and dlp_5'_rev (TTTTGCGGCCGCATGGTTGTCGGGTGTTATTAAATCGG), or dlp_3'_for (TTTTTCTAGATGTCCGATATTATATACCAATGGC) and dlp_3'_rev (TTTTCTCGAGCCAACGATGCTCTACTGTATGC) and cloned into vector pHD-DsRed-attP using restriction enzymes SphI and NotI or SpeI and XhoI, respectively. Homologous directed repair was achieved by co-injecting gRNA plasmids and the repair donor as described [49].

For both *dally*^{KO}and *dlp*^{KO}, successful genomic integrations were identified by the presence of eye markers (mini-white and dsRed, respectively) followed by Cre-mediated excision of marker cassettes. The integrity of the deletion and attP integration was verified by genomic PCR and subsequent sequencing. The exact sequences at the manipulated loci are depicted in Fig. S3.

Dally and Dlp genomic constructs were generated in the reintegration vector pRIVwhite and incorporated into the attP site of the *dally*^{KO} and *dlp*^{KO} alleles by phiC31/attB integration [48]. The YFP sequence in Dally constructs was inserted after lysine 90. Dally$^{\Delta HS}$ contains serine to alanine amino acid substitutions at positions 549, 569, 573 and 597. Three copies of the influenza hemagglutinin derived HA epitope were inserted after glycine 69 of Dlp.

Immunohistochemistry

Total staining

Wing discs from third instar larvae were dissected and stored temporarily in Phosphate Buffered Saline (PBS) (Gibco) on ice until enough samples were collected. The discs were then fixed in 4% Paraformaldehyde (PFA) in PBS for 30 min on the shaker at room temperature (25°C). After fixation, the discs were rinsed three

606 times quickly with PBS and three times for 15 min with PBS at 4°C. Wing discs were permeabilized in PBST
607 (0.3% Triton-X in PBS) and then blocked in 5% normal goat serum (NGS) in PBST for at least 30 min. Primary
608 antibodies were added in 5% normal goat serum (NGS) in PBST for incubation over night at 4°C. The next
609 day, the primary antibodies were carefully removed and the samples were rinsed three times quickly in PBST
610 and three times 15 min at room temperature in PBST. Discs were incubated in secondary antibody for 2h at
611 room temperature. Afterwards the samples were washed again three times quickly and three times 15 min in
612 PBST at room temperature. After the final washing the PBST was rinsed with PBS, then the PBS was
613 removed completely and the samples were mounted in VECTORSHIELD on glass slides. For HS stainings,
614 wing discs were dissected as described above. After fixation, discs were washed in PBS and blocked in 5%
615 NGS in PBST, then treated with Heparinase III (Sigma-Aldrich) for 1.5h at 37°C. Afterwards the discs were
616 blocked again in 5% NGS in PBST and stained as described above.
617
618 **Extracellular staining**
619 Wing discs from third instar larvae were dissected and stored temporarily in Schneider's Drosophila medium
620 (S2) on ice until enough samples were collected. The discs were then blocked in cold 5% NGS in S2 medium
621 on ice for 10min. The blocking solution was removed carefully and the primary antibody was added for 1h on
622 ice. During the 1h incubation period, the tubes were tapped carefully every 15 min, to make sure the antibody
623 is distributed evenly. After 1h incubation on ice, the antibody was removed and the samples were washed at
624 least 6 times with cold S2 medium and another two times with cold PBS to remove excess primary antibody.
625 Wing discs were then fixed with 4% PFA in PBS for 30min on the shaker at room temperature (25°C). After
626 fixation the protocol continued as described in total stainings.
627
628 **Antibodies**
629 Primary antibodies: rabbit-anti-phospho-Smad1/5 (41D10, Cell Signaling, #9516; 1:200), mouse-anti-Wg
630 (4D4, DSHB, University of Iowa; total staining: 1:120, extracellular staining: 1:120), mouse-anti-Ptc (DSHB,
631 University of Iowa; total staining: 1:40), rat-anti-HA (3F10, Roche, 11867423001; total staining: 1:300,
632 extracellular staining: 1:20), rat-anti-Ollas (L2, Novus Biologicals, NBP1-06713; total staining: 1:300,
633 extracellular staining: 1:20), mouse-anti-HS (F69-3G10, amsbio; 1:100)
634
635 The following secondary antibodies were used at 1:500 dilutions in this study. Goat anti-rabbit IgG (H+L)
636 Alexa Fluor™ 488 (A11008 Thermo Fischer), goat anti-rabbit IgG (H+L) Alexa Fluor™ 568 (A11011 Thermo
637 Fischer), goat anti-rabbit IgG (H+L) Alexa Fluor™ 680 (A21109 Thermo Fischer), goat anti-rat IgG (H+L)
638 Alexa Fluor™ 568 (A11077 Thermo Fischer), goat anti-mouse IgG (H+L) Alexa Fluor™ 568 (A11004 Thermo
639 Fischer), goat anti-rat IgG Fc 488 (ab97089 abcam), goat anti-mouse IgG Fc Alexa Fluor™ 680 (115625071
640 Jackson Immuno Research).
641
642 **Imaging**
643 Samples were imaged using a Leica SP5-II-MATRIX confocal microscope and Leica LAS AF and Images
644 were analyzed using ImageJ. Figures were obtained using Omero and Adobe Illustrator.
645
646 **Quantification of pMad and extracellular staining**
647 From each z-stack image, signal intensity profile along A/P axis was extracted from average projection of
648 three sequential images using ImageJ (v.2.0.0-rc69/1.52p). Each signal intensity profile collected in Excel
649 (Ver. 16.51) was aligned along A/P compartment boundary (based on anti-Ptc staining or pMad staining) and
650 average signal intensity profile from different samples was generated and plotted by the script (wing_disc-
651 alignment.py). The average intensity profile from control and experimental samples was then compared by
652 the script (wingdisc_comparison.py). Both scripts can be obtained from
653 https://etiennees.github.io/Wing_disc-alignment/. To normalize extracellular Dpp against the level of Dally or
654 Dally$^{\Delta HS}$, total signal intensity of extracellular Dpp staining (ExOllas staining) was divided by total GFP
655 fluorescent signal (Dally or Dally$^{\Delta HS}$) around the Dpp producing cells in each wing disc (Fig. 4I, 5C). The
656 resulting signal intensity profiles (mean with SD) were generated by Prism (v.8.4.3(471)). Figures were
657 prepared using Omero (ver5.9.1) and Illustrator (24.1.3).
658
659 **Quantification of adult wing size**
660 The size of each compartment was measured using ImageJ (v.2.0.0-rc69/1.52p) and collected in Excel (Ver.
661 16.51). Scatter dot plots (mean with SD) were generated by Prism (v.8.4.3(471)). Figures were prepared
662 using Omero (ver5.9.1) and Illustrator (24.1.3).
663
664 **Statistics**

All images were obtained from multiple animals ($n > 3$). The experiments were repeated at least two times independently with similar results. Statistical significance was assessed by Prism (v.8.4.3(471)) based on the normality tests. The observed phenotypes were highly reproducible as indicated by the significance of p values obtained by statistical tests.

Acknowledgements

We thank Markus Affolter for his continuous support during the course of this project. We thank Developmental Studies Hybridoma Bank at The University of Iowa for antibodies. Stocks obtained from the Bloomington *Drosophila* Stock Center (NIH P40OD018537) were used in this study. We thank Suzanne Eaton, Manolo Calleja, Gary Struhl, and Gustavo Aguilar for flies. We thank Etienne Schmelzer for scripts for quantification. We would like to thank Bernadette Bruno, Gina Evora, and Karin Mauro for constant and reliable supply with world's best fly food. We thank the Biozentrum Imaging Core Facility for the maintenance of microscopes and support. G.P. is indebted to Annette Neubüser for continuous support and to Daniela Reuter-Schmitt for excellent technical assistance.

Funding

S.M. has been supported by the Research Fund Junior Researchers University of Basel and is currently supported by an SNSF Ambizione grant (PZ00P3_180019). The work in the Pyrowolakis lab was funded by the Deutsche Forschungsgemeinschaft (DFG, German Research Foundation) under Germany's Excellence Strategy (EXC-2189-Project ID 390939984).

References

1. Stapornwongkul, K.S., and Vincent, J.P. (2021). Generation of extracellular morphogen gradients: the case for diffusion. Nat Rev Genet *22*, 393-411. 10.1038/s41576-021-00342-y.
2. Tabata, T. (2001). Genetics of morphogen gradients. Nature reviews.Genetics *2*, 620-630. 10.1038/35084577 [doi].
3. Ashe, H.L., and Briscoe, J. (2006). The interpretation of morphogen gradients. Development (Cambridge, England) *133*, 385-394. 133/3/385 [pii].
4. Rogers, K.W., and Schier, A.F. (2011). Morphogen gradients: from generation to interpretation. Annual Review of Cell and Developmental Biology *27*, 377-407. 10.1146/annurev-cellbio-092910-154148 [doi].
5. Affolter, M., and Basler, K. (2007). The Decapentaplegic morphogen gradient: from pattern formation to growth regulation. Nature reviews.Genetics *8*, 663-674. 10.1038/nrg2166.
6. Matsuda, S., Harmansa, S., and Affolter, M. (2016). BMP morphogen gradients in flies. Cytokine & growth factor reviews *27*, 119-127. 10.1016/j.cytogfr.2015.11.003 [doi].
7. Kicheva, A., and Gonzalez-Gaitan, M. (2008). The Decapentaplegic morphogen gradient: a precise definition. Current opinion in cell biology *20*, 137-143. 10.1016/j.ceb.2008.01.008 [doi].
8. Campbell, G., and Tomlinson, A. (1999). Transducing the Dpp morphogen gradient in the wing of Drosophila: regulation of Dpp targets by brinker. Cell *96*, 553-562. 10.1016/s0092-8674(00)80659-5.
9. Jazwinska, A., Rushlow, C., and Roth, S. (1999). The role of brinker in mediating the graded response to Dpp in early Drosophila embryos. Development *126*, 3323-3334. 10.1242/dev.126.15.3323.
10. Minami, M., Kinoshita, N., Kamoshida, Y., Tanimoto, H., and Tabata, T. (1999). brinker is a target of Dpp in Drosophila that negatively regulates Dpp-dependent genes. Nature *398*, 242-246. 10.1038/18451.
11. Muller, B., Hartmann, B., Pyrowolakis, G., Affolter, M., and Basler, K. (2003). Conversion of an extracellular Dpp/BMP morphogen gradient into an inverse transcriptional gradient. Cell *113*, 221-233. 10.1016/s0092-8674(03)00241-1.
12. Cook, O., Biehs, B., and Bier, E. (2004). brinker and optomotor-blind act coordinately to initiate development of the L5 wing vein primordium in Drosophila. Development *131*, 2113-2124. 10.1242/dev.01100.
13. Sturtevant, M.A., Biehs, B., Marin, E., and Bier, E. (1997). The spalt gene links the A/P compartment boundary to a linear adult structure in the Drosophila wing. Development *124*, 21-32. 10.1242/dev.124.1.21.
14. Schwank, G., Restrepo, S., and Basler, K. (2008). Growth regulation by Dpp: an essential role for Brinker and a non-essential role for graded signaling levels. Development (Cambridge, England) *135*, 4003-4013. 10.1242/dev.025635; 10.1242/dev.025635.
15. Matsuda, S., Schaefer, J.V., Mii, Y., Hori, Y., Bieli, D., Taira, M., Pluckthun, A., and Affolter, M. (2021). Asymmetric requirement of Dpp/BMP morphogen dispersal in the Drosophila wing disc. Nat Commun *12*, 6435. 10.1038/s41467-021-26726-6.
16. Akiyama, T., and Gibson, M.C. (2015). Morphogen transport: theoretical and experimental controversies. Wiley interdisciplinary reviews.Developmental biology *4*, 99-112. 10.1002/wdev.167 [doi].
17. Lin, X., and Perrimon, N. (2002). Developmental roles of heparan sulfate proteoglycans in Drosophila. Glycoconj J *19*, 363-368. 10.1023/A:1025329323438.
18. Nybakken, K., and Perrimon, N. (2002). Heparan sulfate proteoglycan modulation of developmental signaling in Drosophila. Biochim Biophys Acta *1573*, 280-291. 10.1016/s0304-4165(02)00395-1.
19. Yan, D., and Lin, X. (2009). Shaping morphogen gradients by proteoglycans. Cold Spring Harb Perspect Biol *1*, a002493. 10.1101/cshperspect.a002493.
20. Nakato, H., Futch, T.A., and Selleck, S.B. (1995). The division abnormally delayed (dally) gene: a putative integral membrane proteoglycan required for cell division patterning during postembryonic development of the nervous system in Drosophila. Development *121*, 3687-3702. 10.1242/dev.121.11.3687.
21. Khare, N., and Baumgartner, S. (2000). Dally-like protein, a new Drosophila glypican with expression overlapping with wingless. Mech Dev *99*, 199-202. 10.1016/s0925-4773(00)00502-5.
22. Kuo, W.J., Digman, M.A., and Lander, A.D. (2010). Heparan sulfate acts as a bone morphogenetic protein coreceptor by facilitating ligand-induced receptor hetero-oligomerization. Mol Biol Cell *21*, 4028-4041. 10.1091/mbc.E10-04-0348.
23. Belenkaya, T.Y., Han, C., Yan, D., Opoka, R.J., Khodoun, M., Liu, H., and Lin, X. (2004). Drosophila Dpp morphogen movement is independent of dynamin-mediated endocytosis but regulated by the glypican members of heparan sulfate proteoglycans. Cell *119*, 231-244. 10.1016/j.cell.2004.09.031.
24. Fujise, M., Takeo, S., Kamimura, K., Matsuo, T., Aigaki, T., Izumi, S., and Nakato, H. (2003). Dally regulates Dpp morphogen gradient formation in the Drosophila wing. Development *130*, 1515-1522. 10.1242/dev.00379.

745 25. Romanova-Michaelides, M., Hadjivasiliou, Z., Aguilar-Hidalgo, D., Basagiannis, D., Seum, C., Dubois, M.,
746 Julicher, F., and Gonzalez-Gaitan, M. (2022). Morphogen gradient scaling by recycling of intracellular Dpp.
747 Nature *602*, 287-293. 10.1038/s41586-021-04346-w.
748 26. Zhu, Y., Qiu, Y., Chen, W., Nie, Q., and Lander, A.D. (2020). Scaling a Dpp Morphogen Gradient through
749 Feedback Control of Receptors and Co-receptors. Developmental cell *53*, 724-739.e714. S1534-
750 5807(20)30418-4 [pii].
751 27. Bornemann, D.J., Duncan, J.E., Staatz, W., Selleck, S., and Warrior, R. (2004). Abrogation of heparan sulfate
752 synthesis in Drosophila disrupts the Wingless, Hedgehog and Decapentaplegic signaling pathways.
753 Development *131*, 1927-1938. 10.1242/dev.01061.
754 28. Han, C., Belenkaya, T.Y., Khodoun, M., Tauchi, M., Lin, X., and Lin, X. (2004). Distinct and collaborative roles of
755 Drosophila EXT family proteins in morphogen signalling and gradient formation. Development *131*, 1563-1575.
756 10.1242/dev.01051.
757 29. Takei, Y., Ozawa, Y., Sato, M., Watanabe, A., and Tabata, T. (2004). Three Drosophila EXT genes shape
758 morphogen gradients through synthesis of heparan sulfate proteoglycans. Development *131*, 73-82.
759 10.1242/dev.00913.
760 30. Akiyama, T., Kamimura, K., Firkus, C., Takeo, S., Shimmi, O., and Nakato, H. (2008). Dally regulates Dpp
761 morphogen gradient formation by stabilizing Dpp on the cell surface. Dev Biol *313*, 408-419.
762 10.1016/j.ydbio.2007.10.035.
763 31. Kerszberg, M., and Wolpert, L. (1998). Mechanisms for positional signalling by morphogen transport: a
764 theoretical study. J Theor Biol *191*, 103-114. 10.1006/jtbi.1997.0575.
765 32. Kicheva, A., Pantazis, P., Bollenbach, T., Kalaidzidis, Y., Bittig, T., Julicher, F., and Gonzalez-Gaitan, M. (2007).
766 Kinetics of morphogen gradient formation. Science *315*, 521-525. 10.1126/science.1135774.
767 33. Muller, P., Rogers, K.W., Yu, S.R., Brand, M., and Schier, A.F. (2013). Morphogen transport. Development *140*,
768 1621-1638. 10.1242/dev.083519.
769 34. Stapornwongkul, K.S., de Gennes, M., Cocconi, L., Salbreux, G., and Vincent, J.P. (2020). Patterning and growth
770 control in vivo by an engineered GFP gradient. Science *370*, 321-327. 10.1126/science.abb8205.
771 35. Bauer Milena, A.G., Wharton Kristi, Matsuda Shinya, Affolter Markus (2022). Heterodimerization-dependent
772 secretion of BMPs in Drosophila. biorxiv. https://doi.org/10.1101/2022.08.04.502599.
773 36. Han, C., Yan, D., Belenkaya, T.Y., and Lin, X. (2005). Drosophila glypicans Dally and Dally-like shape the
774 extracellular Wingless morphogen gradient in the wing disc. Development *132*, 667-679. 10.1242/dev.01636.
775 37. Franch-Marro, X., Marchand, O., Piddini, E., Ricardo, S., Alexandre, C., and Vincent, J.P. (2005). Glypicans shunt
776 the Wingless signal between local signalling and further transport. Development *132*, 659-666.
777 10.1242/dev.01639.
778 38. Kirkpatrick, C.A., Knox, S.M., Staatz, W.D., Fox, B., Lercher, D.M., and Selleck, S.B. (2006). The function of a
779 Drosophila glypican does not depend entirely on heparan sulfate modification. Dev Biol *300*, 570-582.
780 10.1016/j.ydbio.2006.09.011.
781 39. Wang, X., Harris, R.E., Bayston, L.J., and Ashe, H.L. (2008). Type IV collagens regulate BMP signalling in
782 Drosophila. Nature *455*, 72-77. 10.1038/nature07214.
783 40. Hoffmann, F.M., and Goodman, W. (1987). Identification in transgenic animals of the Drosophila
784 decapentaplegic sequences required for embryonic dorsal pattern formation. Genes Dev *1*, 615-625.
785 10.1101/gad.1.6.615.
786 41. McGough, I.J., Vecchia, L., Bishop, B., Malinauskas, T., Beckett, K., Joshi, D., O'Reilly, N., Siebold, C., Jones, E.Y.,
787 and Vincent, J.P. (2020). Glypicans shield the Wnt lipid moiety to enable signalling at a distance. Nature *585*,
788 85-90. 10.1038/s41586-020-2498-z.
789 42. Schwank, G., Dalessi, S., Yang, S.F., Yagi, R., de Lachapelle, A.M., Affolter, M., Bergmann, S., and Basler, K.
790 (2011). Formation of the long range Dpp morphogen gradient. PLoS Biol *9*, e1001111.
791 10.1371/journal.pbio.100111

792 10.1371/journal.pbio.1001111.
793 43. Kanzaki, S., Takahashi, T., Kanno, T., Ariyoshi, W., Shinmyouzu, K., Tujisawa, T., and Nishihara, T. (2008).
794 Heparin inhibits BMP-2 osteogenic bioactivity by binding to both BMP-2 and BMP receptor. J Cell Physiol *216*,
795 844-850. 10.1002/jcp.21468.
796 44. Entchev, E.V., Schwabedissen, A., and Gonzalez-Gaitan, M. (2000). Gradient formation of the TGF-beta
797 homolog Dpp. Cell *103*, 981-991. 10.1016/s0092-8674(00)00200-2.

798 45. Wartlick, O., Mumcu, P., Kicheva, A., Bittig, T., Seum, C., Julicher, F., and Gonzalez-Gaitan, M. (2011). Dynamics
799 of Dpp signaling and proliferation control. Science (New York, N.Y.) *331*, 1154-1159. 10.1126/science.1200037
800 [doi].
801 46. Vuilleumier, R., Springhorn, A., Patterson, L., Koidl, S., Hammerschmidt, M., Affolter, M., and Pyrowolakis, G.
802 (2010). Control of Dpp morphogen signalling by a secreted feedback regulator. Nat Cell Biol *12*, 611-617.
803 10.1038/ncb2064.
804 47. Norman, M., Vuilleumier, R., Springhorn, A., Gawlik, J., and Pyrowolakis, G. (2016). Pentagone internalises
805 glypicans to fine-tune multiple signalling pathways. eLife *5*, 10.7554/eLife.13301. 10.7554/eLife.13301 [doi].
806 48. Baena-Lopez, L.A., Alexandre, C., Mitchell, A., Pasakarnis, L., and Vincent, J.P. (2013). Accelerated homologous
807 recombination and subsequent genome modification in Drosophila. Development *140*, 4818-4825.
808 10.1242/dev.100933.
809 49. Gratz, S.J., Ukken, F.P., Rubinstein, C.D., Thiede, G., Donohue, L.K., Cummings, A.M., and O'Connor-Giles, K.M.
810 (2014). Highly specific and efficient CRISPR/Cas9-catalyzed homology-directed repair in Drosophila. Genetics
811 *196*, 961-971. 10.1534/genetics.113.160713.

812